Structural and Multidisciplinary Optimization (2022) 65:192
https://doi.org/10.1007/s00158-022-03285-y

RESEARCH PAPER

Multistage rocket preliminary design and trajectory optimization using a multidisciplinary approach

F. M. P. Morgado[1] · A. C. Marta[2] · P. J. S. Gil[2]

Received: 7 June 2021 / Revised: 22 May 2022 / Accepted: 24 May 2022 / Published online: 28 June 2022

Abstract

A procedure for rocket preliminary design was developed using a multidisciplinary coupled approach that simultaneously finds the optimal design and trajectory parameters for a given representative insertion in orbit launch mission. Given the nature of the performance metrics and design space, and the distinct design and trajectory problems, heuristic methods were used in a multilevel design optimization architecture. For the design, a continuous genetic algorithm able to perform parallel optimization was developed and benchmarked. The results were obtained with mass and sizing models, required to estimate the rocket structure, and created using historical data regression. For the trajectory, once defined its assumptions, the optimality equations are deduced and the optimal values are found using a particle swarm optimization. The multidisciplinary optimization procedure was demonstrated by designing a small launch vehicle and comparing it to a state-of-the-art existing rocket. Promising results were obtained in both design and trajectory optimization, with the imposed constraints adequately handled and the optimal rocket preliminary design with appropriate optimal trajectory found with an affordable computational cost.

Keywords Launch vehicle · Coupled approach · Multilevel optimization · Two-point boundary-value problem · Genetic algorithm · Particle swarm optimization

1 Introduction

Space launchers are designed by seeking a certain configuration able to perform a given representative mission, that is, the best possible launcher able to put a certain mass into a certain orbit. Being the best can mean having the smallest structural mass, simplest manufacturing or operation, highest reliability, using the best possible trajectory, or a combination of different constraints or preferences of the organization in charge, usually minimizing cost or a close enough proxy, taking all the various constraints into account.

Designing a rocket is very challenging since safety, reliability, and performance must be considered. A substantial part of the overall launcher development is committed at the conceptual and preliminary design phases, and at least 80% of the life-cycle costs are comprised by the chosen concept (Qazi and Linshu 2006). Therefore, there is much to gain in significantly improve the preliminary design tools of space launchers, leading to better performance or reduced complexity and life-cycle cost.

Rocket optimization implies the interaction of diverse engineering disciplines, which often have conflicting objectives and demand a vast search space to find the global optimum. This calls for the use of multidisciplinary design tools which allow to integrate the constraints inherent to each engineering discipline and to ease the optimal design search process. To this end, multidisciplinary design optimization (MDO) architectures become a central piece in building powerful tools to cope with the mutually dependent features and constraints of such complex machines, making possible to design better rockets.

Among the different MDO algorithms documented in the literature (Martins and Lambe 2013), the multidisciplinary feasible (MDF) is the most common method used for rocket optimization, where the different design disciplines are

Responsible Editor: Gengdong Cheng

✉ A. C. Marta
andre.marta@tecnico.ulisboa.pt

[1] Instituto Superior Técnico, Universidade de Lisboa, Lisbon, Portugal

[2] IDMEC, Instituto Superior Técnico, Universidade de Lisboa, Lisbon, Portugal

merged into a single coupled analysis module and the optimum design found by a single top-level optimizer (Duranté et al. 2004; Rafique et al. 2011; Tsuchiya and Mori 2004). However, the handling of all disciplines by a single optimizer, and corresponding constraints, may produce a very large and complex search space, imposing several requirements such as an appropriate initialization and a good knowledge of the design variable domain to be able to converge (Balesdent 2011). These drawbacks led to the creation of MDO algorithms involving several levels of optimization, such as the collaborative optimization (CO) (Braun and Kroo 1996), the bi-level integrated system synthesis (BLISS) (Sobieszczanski-Sobieski et al. 1998), and the analytical target cascading (ATC) (Kim et al. 2003).

The need for specialized MDO tools for space launch vehicles drove to the development of new methods such as the stage-wise decomposition for optimal rocket design (SWORD) method (Balesdent 2011). While classical MDO methods tackle the trajectory as a whole, the SWORD method decomposes the rocket according to the different stages, which not only significantly improves the computational efficiency of the process to obtain a feasible design but also potentially finds lighter optimal designs.

The computational power growth over the last few decades has enabled the increase of model's fidelity to reality, which is a major issue in MDO methods for aerospace vehicles (Yao et al. 2011). Nonetheless, the usage of high-fidelity models in optimization still implies prohibitive computational costs, making reduced models using metamodeling techniques a reliable and preferable choice for preliminary design. The use of such approximate models, also known as surrogate models, can be sufficient to correctly estimate the design features of the vehicle with the desired accuracy (Simpson et al. 2001).

Another difficulty in optimal design is the choice of the appropriate optimizer. While gradient-based algorithms offer much better convergence rate, thus at a reduced computational cost, they require the problem to contain continuous smooth functions of class C1. Not only that, but depending on the initial guess, they converge to the nearest local optimum. The global optimal solution may then be hard to find due to the large number of variables and constraints and the presence of multiple local minima. These issues are frequently addressed by using heuristic methods to find the optimal design, which by construction are gradient-free, such as genetic algorithms (GA), and can be used to explore the design space and optimize rocket designs, even considering multiple objectives (Bayley et al. 2008; Arias-Montano et al. 2012; do Nascimento et al. 2022). A recent study has concluded that GAs are the most common method used by researchers to tackle both single and multi-objective optimizations for solid rocket motors design optimization, due to its ability to explore large design space in order to discover the global optimum design (Mahjub et al. 2020).

Most literature on rocket optimization addresses only specific, even if important, aspects of the problem, possibly because of the sheer complexity of a rocket vehicle, by both the number of disciplines involved and the number of parts. This makes the full optimization problem challenging, and papers addressing all or almost all aspects are not common although there are a few, e.g., Wei et al. (2019). It is often more productive to test new optimization approaches, e.g., data mining to help the design process (Shu et al. 2016), addressing only a few aspects of the rocket, as some of the above-discussed examples, or develop in-depth studies on specific but important aspects of rocket design, or particular types of vehicles (Zhang et al. 2021). Typical and recent examples are studies addressing propulsion (Hao et al. 2015a, b, 2020; Mahjub et al. 2020; Dresia et al. 2021; Casalino et al. 2021), structure (Chunna et al. 2020), specific systems such as a rocoon (rocket-balloon) (Li et al. 2021), a suborbital single stage (Okninski 2017), or a mixed of disciplines, such as aerodynamics and propulsion (Kanazaki et al. 2017), a booster and trajectory (Federici et al. 2021), or other partial aspects (Maddock et al. 2018). Other aspects can contribute to improve the algorithms by establishing first estimates for the iteration processes inevitably involved in many, if not all, methods, such as estimates for performance in the case of tank jettison Teixeira and Gil (2022).

In contrast to the design problem, where good solutions can be obtained even with approximation models, the trajectory problem requires detailed dynamic governing equations that need to be solved using numerical methods to obtain the optimal vehicle control, making it a key point in launch vehicle design (Betts 1998). Different methods exist to tackle trajectory optimization, ranging from direct methods [e.g., pseudospectral knotting (Ross and Fahroo 2004) and collocation methods (Hargraves and Paris 1987)] to indirect methods using the Pontryagin's Minimum Principle (PMP) (Pontani 2014), where none generally prevails. Some attempts have been done to model rocket trajectories with Taylor series, with mixed results (Campos and Gil 2018, 2020). Pseudospectral methods have been used with success to model the trajectory, with promising results (Garrido and Sagliano 2021).

In this work, we aim to develop a general procedure to design rockets according to given mission specifications, where the tight coupling between structural sizing and optimal trajectory control is desired to obtain the ultimate optimum launch vehicle to perform a particular payload orbit insertion.

The created framework tackles the rocket design optimization and corresponding trajectory optimization as a whole, i.e., at every design iteration, the framework proceeds to perform a trajectory optimization for the resultant feasible rocket designs.

In this framework, the trajectory is similar to an initial value problem (IVP), where the rocket trajectory is integrated from the initial conditions and optimized values obtained from the global optimizer. This approach allows to avoid optimizing the flight phases separately, driving the framework to achieve a global optimum.

Several research works on rocket design optimization treat the trajectory optimization as a black box, resulting a lack of information regarding the optimization process and the coupling between rocket design and trajectory. In this work, the trajectory optimizer has the new capability of choosing the optimal time for the coasting phase, before or during the last stage thrusting phase (minimizing the kick time), in contrast with the commonly used coast phase optimization between stages thrust phases. Additionally, the modularity of our framework enables an easy replacement of the optimizers and disciplinary models in order to accommodate the required accuracy levels and available computational power of the end-user.

A multilevel multidisciplinary architecture is put in place, where a top-level global optimizer is used to avoid local minima. To overcome the expected computational burden of the global optimizer, a custom-developed genetic algorithm with parallel processing capability is used to enhance the process speed. To haste the process, we use relatively simple aerodynamic and mass models to illustrate the process. The accuracy of the solutions using such models is meant to be assessed by comparing our results with existing state-of-the-art rockets.

This paper contains five main sections. Section 2 presents an overview of rocket preliminary design procedure, including the definition of fundamental rocket parameters. In Sect. 3, the rocket models in terms of size, mass, and structure are defined, as well as the trajectory models used in the optimization framework. The developed coupled optimal framework for simultaneous rocket design and trajectory optimization is detailed in Sect. 4, where the overall MDO architecture is laid down, the developed and used optimization algorithms are described, and the choice of the trajectory optimization method is justified. The design and trajectory models used in the developed framework are validated in Sect. 5 using existing launch vehicle data as reference. After gaining confidence with the validated models, a test case is presented in Sect. 6, where a small launch vehicle is designed, for a selected reference mission of another existing launcher, and the obtained design compared to the existing one. The paper ends with a summary of the achievements and final remarks about the work in Sect. 7.

2 Rocket preliminary design

We start our work by providing some background on rocket design, including fundamental concepts such as velocity change, specific impulse, multistaging, and typical design variables (Sects. 2.1, 2.2). Then we proceed to define the general coupled rocket preliminary design and trajectory optimization procedure, independently of the particular rocket and trajectory models employed in our launch vehicle design (Sect. 2.3).

2.1 Rocket fundamentals

The ability of a rocket to deliver a payload with a certain mass into a desired orbit, with a particular orbital velocity, can be measured by the change in velocity produced by its propulsion against external forces. This velocity change is given by the Tsiolkovsky rocket equation (Tewari 2007),

$$\Delta V = V_f - V_0 = v_e \ln \frac{m_0}{m_f}, \tag{1}$$

where ΔV is the maximum velocity change, V_f and V_0 are, respectively, the final and initial velocities (the latter being zero at launch), v_e is the effective exhaust velocity, m_0 is the initial rocket mass and m_f is the final rocket mass. The rocket total mass can be divided into three main components: the desired payload to launch, the propellant needed for the launch, and the vehicle structure including engines and control system.

During launch, a rocket is subjected to external forces, the most important being drag and gravity, that can be expressed in terms of velocity losses (since they diminish performance), transforming the required mission ΔV into (Turner 2008)

$$\Delta V = \Delta V_{\text{orbit}} + \Delta V_{\text{drag}} + \Delta V_{\text{gravity}}, \tag{2}$$

where ΔV_{orbit} is the velocity required for orbital insertion and ΔV_{drag} and $\Delta V_{\text{gravity}}$ are the losses due to drag and gravity, respectively. Losses due to trajectory correction steering and other forces are much smaller so, with the exception of fully detailed dynamics simulations, they are usually neglected. By definition, the gravity loss is

$$\Delta V_{\text{gravity}} = \int_{t_0}^{t_f} g \sin\gamma \, \mathrm{d}t, \tag{3}$$

where g represents the acceleration of gravity and γ the flight path angle. The initial time t_0 and final time t_f are the boundaries of the time interval to calculate the velocity loss, usually comprising the entire flight duration. The drag loss is given by

$$\Delta V_{\text{drag}} = \int_{t_0}^{t_f} \frac{D}{m} \mathrm{d}t, \tag{4}$$

where D is the drag force, and m the instantaneous rocket mass.

Chemical rocket thrust is the result of the change of the gas momentum due to the transformation of heat into kinetic energy, which is defined as

$$T = \dot{m}\, V_e + A_e(p_e - p_a) = \dot{m}\, v_e\,, \tag{5}$$

where $\dot{m}$ is the mass flow rate through the nozzle, V_e is the exhaust velocity, A_e is the exit nozzle area, and p_e and p_a are the exit nozzle pressure and atmospheric pressure, respectively. Since the engine performance depends on the local atmospheric pressure, its nozzle can be optimized for the most favorable point that depends on the trajectory.

To compare different propellants and engines, the specific impulse I_{sp} is usually used, describing the total impulse delivered per unit weight of propellant,

$$I_{\text{sp}} = \frac{T}{\dot{m}\, g_0} = \frac{v_e}{g_0}\,, \tag{6}$$

where g_0 is the acceleration of gravity at the Earth's surface. The specific impulse of modern solid propellant engines can be up to 250 s (e.g., ammonium nitrate composite propellant), whereas liquid engines can reach 450 s (e.g., LH2/LOX propellant) thanks to their higher energy density content. Historically, solid propellant engines have been mainly used for first stage and boosters, as it provides high thrust-to-weight ratio with a simple design, therefore being highly cost-effective. For upper stages, liquid propellant engines are more commonly used due to their ability to throttle and restart ignition.

2.2 Staging

Since most of the mass of the rockets is propellant, a considerable part of the structure is used to transport it. Hence, it is highly advantageous to consider multistage concepts, which discard stages when empty of fuel in order to reduce the overall rocket mass and, thus, propellant needs.

The arrangement of stages can be serial, parallel, or a mix of both. In serial staging, the stages are stacked upon each other and the thrust is provided by one stage at a time. This is the typical arrangement for small to medium rockets and, as such, it will be considered in our work.

For a N-stage rocket, let the kth stage mass be

$$m_k = m_{p,k} + m_{s,k}\,, \tag{7}$$

where m_p and m_s represent the propellant and the structural masses, respectively.

Dimensionless mass ratios are usually used to ease the analysis. The structural ratio is a dimensionless measure of how much of the stage mass is structural. The stage structural mass comprises only the dry mass, thus the structural ratio of the kth stage is defined as

$$\sigma_k = \frac{m_{s,k}}{m_k}\,. \tag{8}$$

For a multistage rocket with a total of N serial stages, the ideal velocity change is the sum of the individual stage contributions, so the Tsiolkovsky's rocket equation (1) can be rewritten as

$$\Delta V = \sum_{k=1}^{N} v_{e,k} \ln \frac{m_{0,k}}{m_{f,k}}\,, \tag{9}$$

where $m_{0,k}$ is the sum of the kth stage mass and payload mass, and $m_{f,k}$ is the sum of the kth stage structural mass and payload mass.

The parameters just described constitute the most fundamental high-level factors in rocket design, but a rocket is considerably more complex than that. The machine has to be built in a functioning way with a structure that must withstand until the end of the launch, subject to vibrations and the effects of the atmosphere, winds and other disturbances, that are different for different angles-of-attack, and high-speed heating. The dynamics must be appropriate and the trajectory must assure safety and optimal performance. All these and more physical parameters and effects must be taken into account and constrain the rocket design.

Modeling complex machines always imply some simplification of the reality. During the design phase, when different possibilities need to be explored, the use of high-fidelity models to accurately describe the problem require considerable time and computational resources so simplifying assumptions have to be made. The idea is to capture the fundamental features and behavior of the system, the so-called drivers of the system (Wertz and Larson 1999), within a certain degree of uncertainty and error at an affordable computational cost. This can be explored in a framework of variable degree of model complexity, in which low-fidelity models can be used first to broadly explore the phase space and narrow the possibilities, and then more accurate, but more complex and costly models, can be used to increase the accuracy. It is in this context that we develop a procedure to apply this idea for preliminary design of rockets, as described next.

2.3 General procedure

The design of a rocket must start by knowing what it is designed for, typically to have the capability to put a certain payload into a specific orbit, subject to high-level constraints such as price or availability of engines. Once the goal and main constraints are known, the design can proceed to try to obtain the best rocket.

Usually, a lighter rocket is better because it allows a larger payload to be launched or the vehicle to be smaller

and less expensive. The main difficulty is the tight coupling that exists in both the vehicle design and the launch trajectory in terms of vehicle weight: on the one hand, the structural weight and the required propellant weight are mutually dependent; on the other hand, the selected trajectory impacts the propellant consumption, thus also influences the vehicle weight. This implies an iterative design procedure between the two main modules: the structures module and the trajectory module. These models can be of variable fidelity levels to define the mass and structure, and the optimal trajectory, depending on the desired solution accuracy and the computational resources.

Our approach divides the general design loop in different steps, as illustrated in Fig. 1, for the coupled vehicle and trajectory optimization.

Starting from the goal, we first determine which parameters will be subject to optimization and which are kept fixed. The general configuration of the rocket must then be defined, including the number of stages, the usage of boosters, and the type of engines, eventually resulting in additional design constraints. For example, the designer may want to use an existent propulsion system, thus fixing thrust, specific impulse, mass, and other characteristics. Other parameters can also be fixed or bound constrained, if required. For example, if the diameter of the rocket is to be optimized but has to be limited due to the launch platform size limitations, then it must be included as an additional constraint before the structural definition.

Next, we must estimate the required ΔV to reach the goal using the rocket equation (1). This involves estimating the losses from gravity (3) and drag (4). To do that, some heuristics or, if a trajectory was already simulated, values of the previous loop can be used. Other required parameters can also be estimated or defined when required, such as the total estimated ΔV distribution among the different stages in terms of mass ratios.

At this point, all inputs that define the structure must be set and the structures module will determine the mass and sizing of the structure of the stages, boosters, and connectors. This is an iterative process as the required size and mass to meet the imposed ΔV for stage and the required propellant are mutually dependent. First, we start from a conservative structural factor and use a model to size the mass and structure. Then, the structural factor is updated by the model and the process is iterated until convergence.

After reaching that provisional rocket design, the trajectory computation can be run. The path must meet the defined goal, while being compatible with certain constraints,

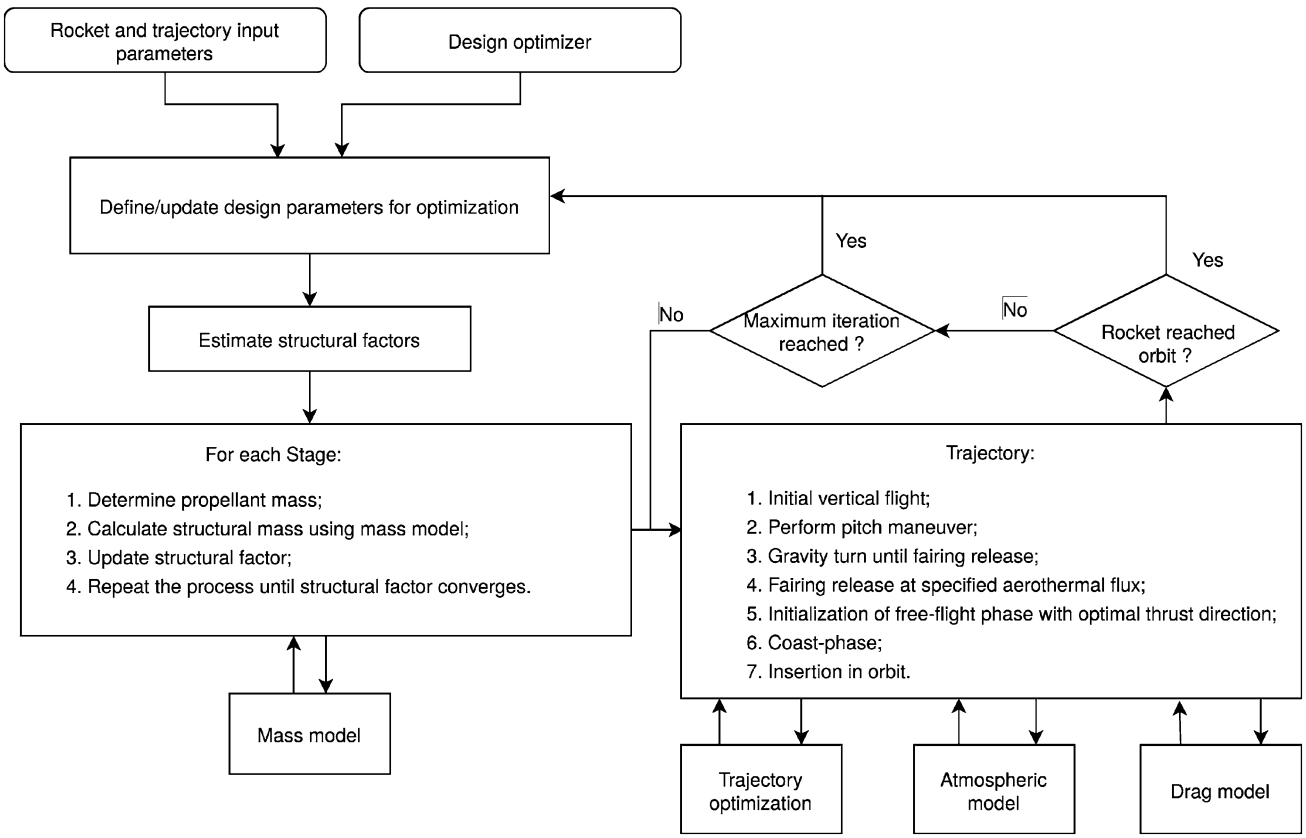

Fig. 1 General coupled rocket preliminary design and trajectory optimization procedure

typically orbit insertion at a specific height and velocity. Since the trajectory followed by the launcher has a major influence on its performance and it is strongly dependent on the design of the vehicle, we opt to perform the vehicle design and its trajectory optimization simultaneously, albeit at multilevel.

Before starting the search for an optimal trajectory, the implemented design constraints are checked for violations. If any constraint is violated, such as the thrust-to-weight ratio, the rocket mass suffers a penalty and the individual design evaluation ends without performing the trajectory simulation. Other heuristics can also be included to limit the phase space and avoid unnecessary effort. For example, our rocket ΔV is limited to $8.5\,\mathrm{km/s} \leq \Delta V \leq 10\,\mathrm{km/s}$, since low Earth orbit speed is less but near 8 km/s and velocity losses are expected to be at the most 2 km/s (Darrin and O'Leary 2009) for an efficient rocket. Excessive ΔV reflects more capacity than the design requirement, while insufficient ΔV means the rocket is unable to reach the specified orbit. Both constraints diminish the search space size, facilitating the search for feasible designs.

Following the estimation of the rocket mass and satisfaction of the design constraints, the trajectory is calculated and a search for an efficient trajectory starts. As in the case of the rocket design, low-fidelity models and assumptions may also be used for the rocket dynamics and atmosphere to reduce the computational cost. The trajectory is then optimized and the required orbit insertion condition is checked. If the propellant is not enough or if too much remain, then the vehicle design is not coupled optimal, so the information is updated (e.g., losses) and the procedure loops back to the structure module to search for better parameter values.

3 Rocket sizing and trajectory models

Following the general coupled optimization procedure described in Sect. 2.3, we now present the details about the actual rocket model (Sect. 3.1) and trajectory model (Sect. 3.2) used in our work. This includes the specific assumed hypotheses and imposed constraints. It should be noted that our procedure is applicable to all type of rockets, regardless of the number/existence of stages and/or boosters, propellant type, and structural material. Naturally, their choices will impact the appropriate discipline models to be used.

3.1 Sizing, mass, and structural model

3.1.1 Stages dry mass and sizing estimation

The total vehicle mass includes the structural mass, propellant mass, and payload. As mentioned in Sect. 2.3, since the propellant mass depends on the structural mass, an iterative process is needed for the mass estimation, starting from an initial guess of the structural ratio.

For the simulations performed in this work, we considered the liquid engine mass m_{LE} decomposed in its components (Frank et al. 2015),

$$m_{\mathrm{LE}} = m_{\mathrm{tc}} + m_{\mathrm{st}} + m_{\mathrm{tankO}} + m_{\mathrm{tankF}}\,, \tag{10}$$

where m_{tc}, m_{st}, m_{tankO} , and m_{tankF} are the thrust chamber, support structure, oxidizer tank, and fuel tank mass, respectively. The thrust chamber mass, composed by the propellant injectors, igniter, combustion chamber, exhaust nozzle, and cooling system, can be empirically estimated by performing a least-squares regression on historical data of engines maximum vacuum thrust T (Humble 1995) as

$$m_{\mathrm{tc}} = \frac{T}{g_0\,(25.2\log T - 80.7)}\,. \tag{11}$$

Similarly, the support structure mass is also empirically estimated from historical data (Rohrschneider 2002),

$$m_{\mathrm{st}} = 0.88 \times 10^{-3} \times (0.225T)^{1.0687}. \tag{12}$$

We consider thin-wall cylindrical tanks with semi-spherical ends for both the oxidizer and the fuel, being their masses given by

$$m_{\mathrm{tank}} = \rho_{\mathrm{mat}}\left(A_{\mathrm{c}} t_{\mathrm{c}} + A_{\mathrm{s}} t_{\mathrm{s}}\right), \tag{13}$$

where ρ_{mat} is the material density, A_{c} and A_{s} are the surface area of the cylindrical and spherical sections, respectively, and t_{c} and t_{s} are the wall thickness of the cylindrical and spherical sections, respectively. The required wall thickness is deduced from the calculation of the burst pressure p_{b}. To calculate the pressure burst, an empiric equation (Humble 1995) with a safety factor term is used (Frank et al. 2015)

$$p_{\mathrm{b}} = \eta_{\mathrm{s}}\lambda_{\mathrm{b}}\left(10^{-0.10688\,(\log V_{\mathrm{tank}} - 0.2588)}\right) \times 10^{6}, \tag{14}$$

where V_{tank} is the required tank volume. The safety factor η_{s} is set to 2 and the ratio between the maximum expected operating pressure and the tank pressure λ_{b} is set to 1.2, as recommended in Frank et al. (2015). The volume of each tank is determined by

$$V_{\mathrm{tank}} = \frac{m_{\mathrm{O/F}}}{\rho_{\mathrm{O/F}}}, \tag{15}$$

where $m_{\mathrm{O/F}}$ and $\rho_{\mathrm{O/F}}$ are the oxidizer/fuel mass and density, respectively.

The stage dry mass includes both the liquid engine and the outer-shell,

$$m_{\text{stage}} = m_{\text{LE}} + \rho_{\text{mat}} L_{\text{stage}} \pi \left[\frac{D_{\text{stage}}^2}{4} - \left(\frac{D_{\text{stage}}}{2} - t_{\text{w}} \right)^2 \right], \tag{16}$$

where t_{w} is the wall thickness and L_{stage} and D_{stage} are the stage length and diameter, respectively.

Assuming a stacked tank configuration, the length of the stage is calculated as

$$L_{\text{stage}} = L_{\text{tc}} + L_{\text{tankO}} + L_{\text{tankF}}\,, \tag{17}$$

where L_{tc} is the thrust chamber length and L_{tankO} and L_{tankF} are the oxidizer and fuel tank lengths, respectively. The thrust chamber length can be empirically estimated from the historical data (Frank et al. 2015) as

$$L_{\text{tc}} = 3.042 \times 10^5 T + 327.7 \tag{18}$$

and the tank length is calculated geometrically from

$$L_{\text{tank}} = D_{\text{tank}} + \frac{V_{\text{tank}} - \frac{4}{3}\pi \left(D_{\text{tank}}/2 \right)^3}{\pi \left(D_{\text{tank}}/2 \right)^2}. \tag{19}$$

3.1.2 Buckling constraints

Rockets have typically a cylindrical wall structure as thin as possible to minimize mass but strong enough to withstand the loads it is subject to. During the thrusting phase, a rocket experiences substantial inertial forces, resulting in high compression loads. These loads in such thin walls are prone to induce buckling, thus play an important role in the structural sizing.

Buckling happens when the compression loads reach a critical value, after which the structure becomes unstable and fails. From the linearized buckling equations for a thin elastic cylindrical shell of thickness t and radius R, the critical stress is given by (Koiter 1945)

$$\sigma_{\text{crit}} = \frac{E}{\sqrt{3\left(1 - \nu^2\right)}} \left(\frac{t}{R} \right), \tag{20}$$

where E is the material Young's modulus and ν is the Poisson's ratio. The critical stress in (20) is independent of the structure length L but it is only valid for intermediate length shells ($0.2 \leq L/R \leq 20$), which is found appropriate for the rocket stages considered in this work. Assuming constant stress on the structure cross-section, the critical load can then be computed as

$$L_{\text{crit}} = \sigma_{\text{crit}} \pi \left[R^2 - (R - t)^2 \right]. \tag{21}$$

We apply a safety factor of 1.5 to this criterion, above the minimum value of 1.4 typically used for rocket structural walls (Bernstein 2011).

Recalling Fig. 1, after the trajectory optimization, the algorithm verifies if the rocket has successfully reached orbit. It also verifies if the axial load is below the critical load (21) and if the maximum dynamic pressure affecting the rocket is below the maximum admissible value of $q \leq 55,000\,\text{N}/\text{m}^2$ to guarantee the structural integrity during the flight (Civek 2014), penalizing the mass if these constraints are violated.

3.2 Trajectory model

3.2.1 Trajectory phases

Space launchers must reach a specific orbit by following a certain ascent trajectory, compliant with the constraints. To minimize the required structural mass, the trajectory should be such that the lateral forces are reduced, due to either the vehicle mass distribution or the dynamic pressure.

Most space launchers lift-off from a launch pad on the ground and try to quickly exit the atmosphere to reduce drag losses. However, a steep ascent leads to more gravity losses as more energy is needed to overcome gravity. Typically, space launchers have an initial very steep trajectory phase, to cope with winds and other perturbations, that can be considered approximately in a vertical plane maintaining a zero angle of attack to keep most forces along the vehicle axis, apart small deviations due to maneuvering. The curve that follows should be such that the transverse component of gravity is mostly compensated by the centrifugal force, thus limiting the transverse force. Thrust can in general also vary, depending on the specific engine technology used, to better cope with drag. Following these general guidelines, the trajectory can be fully optimized.

With that in mind, the flight sequence adopted in this work follows the strategy illustrated in Fig. 2, which includes some simplifications to limit the dimension of the phase space and can be divided into three main phases.

The first phase is the vertical lift-off that lasts the time required to achieve a certain altitude that can be adjusted and optimized.

The second phase is the gravity turn that is initiated with the pitch over maneuver that induces a small pitch that establishes the initial flight path angle, where the trajectory is such that the transverse component of gravity is exactly compensated by the centrifugal force due to the curved trajectory, while still maintaining an almost null angle of attack throughout the atmosphere, minimizing the transverse aerodynamic stress (Turner 2008). The gravity turn maneuver ends when the calculated aerothermal flux $\phi = \frac{1}{2}\rho V^3$, being ρ the local atmospheric density and V the speed (Tewari 2007), is below a specified value typically around $1135\,\text{W}/\text{m}^2$ (Balesdent 2011). The equation assume a free

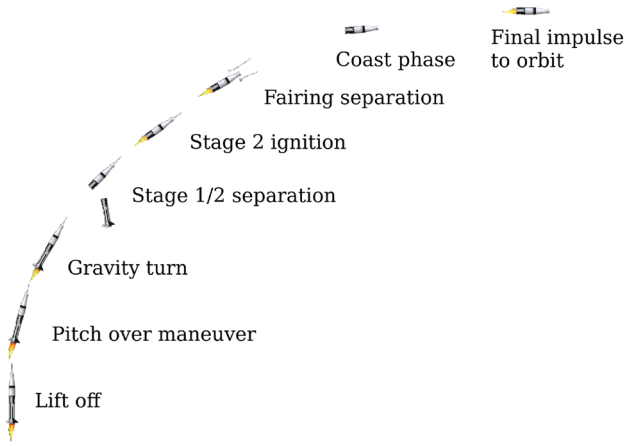

Fig. 2 Typical flight sequence of a space launcher

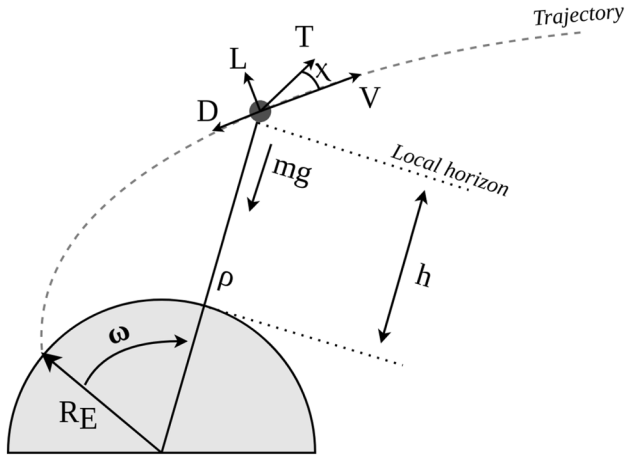

Fig. 3 Rocket state variables and forces during flight

molecular flow through a plane perpendicular to the velocity direction, as a function of dynamic pressure and velocity.

At the end of the gravity turn, aerodynamic forces are negligible, the shroud protecting the payload is dropped off and the rocket can start correcting the trajectory, starting the third, free-flight, phase. The free-flight phase is treated as a two-point boundary-value problem (TPBVP), in which the vehicle initial state corresponds to the end of gravity turn and its final state to the desired orbit insertion, specified by altitude, velocity, and flight path angle, and the vehicle maneuvers to minimize the consumed propellant.

3.2.2 Vehicle dynamics

In this work, we considered the rocket to be a variable-mass rigid body flying in a 2-D plane model, as illustrated in Fig. 3 (Sforza 2011), for which the forces acting in the rocket are applied at the center of mass during flight.

The rocket's active stage produces a constant thrust T with an angle χ with respect to the velocity vector $\overrightarrow{V}$. In the context of trajectory analysis and optimization, the thrust direction can be assumed as always being aligned with the vehicle longitudinal axis. Thus, it is equivalent to the angle of attack α ($\chi = \alpha$).

The force of gravity applied on the vehicle is mg, where m is the vehicle mass and g is the local acceleration of gravity, pointing to the center of the Earth.

Until the end of the gravity turn maneuver, the drag force is not negligible and it has to be taken into account, being estimated from an appropriate aerodynamic model (see Sect. 3.2.3). The lift force L is neglected as it is held closely to zero during the powered ascent through the atmosphere (Curtis 2015).

The Coriolis and centrifugal acceleration due to the Earth rotation are also neglected during trajectory simulation (Reilly 1979). The main effect of Earth rotation is the imposition of a initial velocity to the rocket in the inertial frame of reference. To obtain the rocket velocity in the inertial frame of reference, this contribution can be added to the rocket velocity to the rotational frame of reference at any given time, such that

$$\overrightarrow{V_i} = \overrightarrow{V_0} + \overrightarrow{V_r}, \tag{22}$$

where $\overrightarrow{V_i}$ and $\overrightarrow{V_r}$ are the rocket velocity in the inertial and rotational reference frame, respectively, and $\overrightarrow{V_0}$ is the velocity contribution due to Earth rotation. This contribution depends on the launch site latitude and it is determined from the Earth angular velocity.

A reference system attached to the Earth, with origin at its center and angular velocity ω, is used to better describe the rocket motion for a near-equatorial orbit (Pontani 2014), as shown in Fig. 3. The equations of motion of the vehicle in the tangential and normal directions are, respectively (Sforza 2011),

$$\dot{V} = \frac{T}{m}\cos\alpha - \frac{D}{m} - g\sin\gamma\,, \tag{23a}$$

$$V\dot{\gamma} = -\left(g - \frac{V^2}{R_\mathrm{E}+h}\right)\cos\gamma + \frac{T}{m}\sin\alpha\,, \tag{23b}$$

where γ is the flight path angle, T is the rocket thrust, V is the rocket velocity, m is the instantaneous rocket mass, D is the drag force, and α is the angle of attack.

The rate of change of the downrange distance x and altitude h of the vehicle are given by

$$\dot{x} = \frac{R_\mathrm{E}}{R_\mathrm{E}+h}V\cos\gamma\,, \tag{24a}$$

$$\dot{h} = V \sin\gamma\,, \tag{24b}$$

where R_E is the radius of the Earth (Sforza 2011).

The trajectory is then calculated using a fourth-order explicit Runge–Kutta method (RK4) (Tewari 2007) to generate the numerical solution. This includes the gravity turn part, as this phase was corrected with the drag force, not considered in simpler models.

During the trajectory time-marching scheme, some vehicle flight requirements are enforced. During the gravity turn and free-flight, the stages' burn time and acceleration are monitored. When using liquid stages, our algorithm limits the rocket acceleration to $a \leq 5g_0$ to protect the payload by throttling down the engines. When the propellant tank is depleted, staging occurs to release useless mass. The condition chosen to end the gravity turn was the aerothermal flux of the free molecular flow to decrease below the nominal value of 1135 $\mathrm{W/m^2}$ (Balesdent 2011), where the fairing can safely be jettisoned since aerodynamic loads will not damage the payload further this point. This condition allows the rocket to jettison the fairing at altitudes typically between 100 and 120 km, which are common for rockets (Meseguer et al. 2012). Afterward, the free-flight phase starts and optimal control is initiated for the rocket to follow the optimal trajectory. The rocket continues to thrust until the initialization of the coast phase. Afterward, the thrusting phase lasts until the specified burn time of the last stage Δt_T is reached. The rocket final position is then assessed by the optimizer to tune the optimization variables (see Sect. 4.2.2).

3.2.3 Aerodynamic and atmospheric models

The aerodynamic drag force is expressed as $D = C_D \frac{1}{2}\rho S V^2$, where v is vehicle flight speed, ρ is the air density, and S is a characteristic surface area. The drag coefficient C_D is approximated as a function of only the Mach M and Knudsen Kn numbers using the Missile DATCOM software for different nose geometries (Ritter 2012). In the hypersonic regime, C_D becomes almost invariant with M after a critical Mach number, generally between 4 and 6 (Kliche et al. 2011), as observed in Fig. 4.

Since the DATCOM software does not use the Knudsen number in the estimates and only considers continuum flow, we correct C_D as (Tewari 2011)

$$C_D = \begin{cases} C_{Dc}(M) & \text{if } Kn < Kn_c \\ C_{Dfm} & \text{if } Kn > Kn_f \\ C_{Dc} + (C_{Dfm} - C_{Dc})\left[\frac{1}{3}\log_{10}(A\,Kn) + B\right] & \text{otherwise}\,, \end{cases} \tag{25}$$

where $C_{Dc}(M)$ is the drag coefficient in the continuum flow limit, function of the Mach number, and nose geometry, and

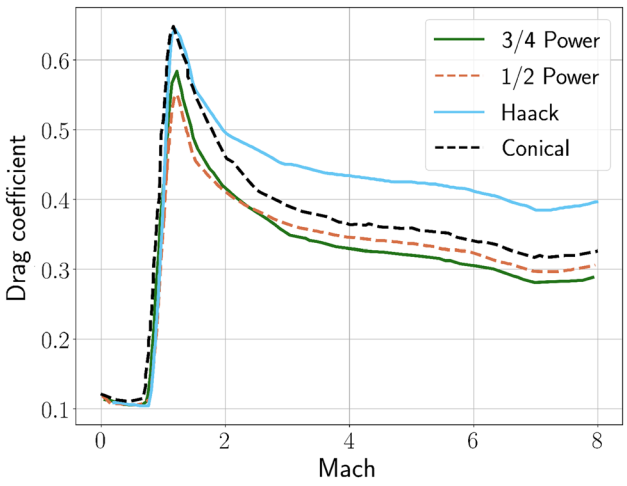

Fig. 4 Influence of Mach number in drag coefficient [based on Ritter (2012)].

C_{Dfm} is the drag coefficient in the free molecular limit given by the cold-wall approximation (Chambre and Schaaf 2017),

$$C_{Dfm} = 1.75 + \frac{\sqrt{\pi}}{2s}\,, \tag{26}$$

where $s = \frac{V}{\sqrt{2RT}}$ denotes the molecular speed ratio, with T being the air temperature and R being the air specific gas constant. The Knudsen numbers Kn_c and Kn_f represent the Knudsen limits of continuum flow and free molecular flow, respectively, which depend exclusively on the vehicle geometry. The Knudsen number is given by the ratio of the molecular mean free path length and a characteristic length (typically the nose radius of the last stage), $Kn = \lambda/L$. The constants (A, B) are selected to perform a smooth bridging between the continuum and free molecular flow regimes. In this work, the chosen constants are $A = 2$ and $B = 0.5113$ (Tewari 2007).

In contrast to our approach, it should be noted that some legacy works do not use trajectory models nor drag models to compute the losses by Eqs. (3) and (4) and use instead a preliminary estimate of 1.5–2 km/s, mainly due to gravity, that is found to be reasonable in many cases (Darrin and O'Leary 2009).

The atmospheric properties vary with the altitude and affect the vehicle performance. The atmospheric temperature, density, and pressure are modeled by interpolating the data provided in the 1976 US Standard atmosphere. During atmospheric flight, the flow regimes vary from continuum to free molecular flow. The tangible atmosphere ends when the vehicle enters the free molecular regime ($Kn \geq 10$), which occurs near the Kaŕmán line ($h \approx 100$ km).

4 Coupled optimal design and control

The rocket design and trajectory models described in Sect. 3 are used in the development of our coupled optimization framework using an MDO approach. To that end, this section starts by posing the optimal trajectory and control problem (Sect. 4.1), followed by the description of the coupled optimization architecture and the developed and selected optimization algorithms (Sect. 4.2). The actual implemented design framework is then described in detail, with emphasis on the main evaluation modules and their data flow (Sect. 4.3).

4.1 Trajectory optimal control

Historically, the numerical trajectory solution has been pursued using different methods and can be divided into indirect methods, where the necessary and sufficient conditions for optimality are analytically constructed and solved numerically, and direct methods, where the optimization problem is converted into a nonlinear programming (NLP) problem (Betts 1998).

In general, direct methods are more robust in terms of convergence, even with poor initial guesses. Despite being harder to initialize, we chose an indirect method in our work because it provides more accurate results, which is deemed critical for aerospace applications. Indirect methods use optimal control theory to transform an optimization problem into a Two-Point Boundary-Value Problem (TPBVP) by introducing Lagrangian multipliers, also known as adjoint variables. To mitigate the hard initialization of the indirect method, a PSO was used to search the optimal trajectory parameters, as it is not only capable of providing the initial values of the adjoint variables for the optimal control, but also to optimize the trajectory parameters not related to control, while enforcing the optimality conditions (Conway 2010) (refer to Sect. 4.2.2).

The indirect method is only applied during the free-flight phase, after the jettison of the fairing. Prior to the jettison, there is no control on the rocket, as it only requires to performs a gravity turn. The gravity turn starts at the specified time of $t = 3$ s due to a pitch maneuver optimized by the PSO heuristic search. Additionally, the PSO optimizes the duration of the last stage thrusting time and the starting time and duration of the coast phase, restricted to occur during the last stage thrusting.

The optimal controls for the optimized trajectory are found by using an Hamiltonian function and applying the Pontryagin's Minimum Principle (PMP) (Pontryagin 1987). The derivation of the adjoint equation, the control equation, and the boundary condition (transversality conditions) function from the Hamiltonian function are briefly described next.

The indirect method tries to minimize the objective function while complying with the optimality constraints. Common objectives used in trajectory optimization are flight time and propellant consumption. In this work, we consider constant propellant mass flow so these two metrics are equivalent. As such, the objective function J in the last phase of the trajectory is the impulse duration for orbital injection,

$$J = t_{\mathrm{f}} - t_{\mathrm{cf}}\,, \tag{27}$$

where t_{f} and t_{cf} are the final flight time and the final coast time, respectively. Since we are considering staging and coasting, there will be discontinuities in mass and thrust through the flight. To handle these discontinuities, the trajectory is split into flight arcs.

We define the Hamiltonian function for each flight arc as

$$H = L + \boldsymbol{\lambda}^T \boldsymbol{f} = \lambda_x \dot{x} + \lambda_h \dot{h} + \lambda_V \dot{V} + \lambda_\gamma \dot{\gamma} \tag{28}$$

where L is the Lagrangian of the system and $\boldsymbol{\lambda}^T \boldsymbol{f}$ is the adjoint or costate variables conjugate to the state equations (Betts 1998). In our problem, λ_x, λ_h, λ_V , and λ_γ are the adjoint variables associated with the corresponding state equations $\dot{x}$, $\dot{h}$, $\dot{V}$, and $\dot{\gamma}$ that are the equations of motions (23) and (24).

The adjoint differential equations are deduced using

$$\frac{\mathrm{d}\lambda}{\mathrm{d}t} = -\left(\frac{\partial H}{\partial x}\right)^T, \tag{29}$$

where x represents the state variables. This leads to the set of conditions to be satisfied to minimize the Hamiltonian,

$$\dot{\lambda}_x = 0\,, \tag{30a}$$

$$\dot{\lambda}_h = \frac{1}{(R_{\mathrm{E}}+h)^2} V \lambda_\gamma \cos\gamma - \left(2\mu_{\mathrm{E}}\lambda_V \sin\gamma + \frac{2\mu_{\mathrm{E}}\lambda_\gamma \cos\gamma}{V}\right)\frac{1}{(R_{\mathrm{E}}+h)^3}, \tag{30b}$$

$$\dot{\lambda}_V = -\lambda_h \sin\gamma - \lambda_\gamma\left[\cos\gamma\left(\frac{1}{R_{\mathrm{E}}+h} + \frac{\mu_{\mathrm{E}}}{(R_{\mathrm{E}}+h)^2 V^2}\right) - \frac{T}{m}\frac{1}{V^2}\sin\alpha\right], \tag{30c}$$

$$\dot{\lambda}_\gamma = -V\lambda_h \cos\gamma + \mu_{\mathrm{E}}\lambda_V \frac{\cos\gamma}{(R_{\mathrm{E}}+h)^2} + \lambda_\gamma \sin\gamma\left(\frac{V}{(R_{\mathrm{E}}+h)} - \frac{\mu_{\mathrm{E}}}{(R_{\mathrm{E}}+h)^2 V}\right), \tag{30d}$$

where μ_{E} is the gravitational parameter of the Earth. Since the costate equations (30) are homogeneous in λ, the costate

initial values can be sought in the interval $-1 \leq \lambda_k \leq 1$ to reduce the search space.

The optimal control is determined by minimizing the Hamiltonian with respect to the control variables u,

$$\left(\frac{\partial H}{\partial u}\right)^T = 0\,, \tag{31}$$

and by assuring the Legendre–Clebsch condition ($\frac{\partial^2 H}{\partial u^2}$ has to be positive semi-definite). Our control variable is the rocket angle of attack α, assumed to be equal to the thrust deflection χ (Pallone et al. 2016), which can be written in terms of the adjoint and state variables through the PMP,

$$\alpha = \arg\min_{\alpha} H\,, \tag{32}$$

which is the equivalent to solve

$$\frac{\lambda_\gamma}{V}\sin\alpha + \lambda_V \cos\alpha = 0\,, \tag{33}$$

with

$$\sin\alpha = -\frac{\lambda_\gamma}{V}\sqrt{\left[\left(\frac{\lambda_\gamma}{V}\right)^2 + \lambda_V^2\right]} \tag{34a}$$

and

$$\cos\alpha = -\lambda_V\sqrt{\left[\left(\frac{\lambda_\gamma}{V}\right)^2 + \lambda_V^2\right]}, \tag{34b}$$

to verify the PMP.

Finally, the transversality conditions can be deduced by solving

$$(\boldsymbol{\Phi}_t + H)|_{t=t_f} = 0\,, \tag{35}$$

where $\boldsymbol{\Phi}$ is the boundary condition function, given by

$$\boldsymbol{\Phi} = J + \boldsymbol{\nu}^T\boldsymbol{\Psi}(x_f)\,, \tag{36}$$

where $\boldsymbol{\nu}^T\boldsymbol{\Psi}(x_f)$ is the time-independent adjoint variable conjugate to the boundary conditions. Due to the Weierstrass–Erdmann corner conditions, the adjoint variables are continuous across successive flight arcs. As we consider that the vehicle must reach a desired orbit, with a specified insertion point, we prescribe the final state values for altitude h', velocity V', and flight path angle γ', resulting for the terminal boundary constraints

$$\boldsymbol{\Psi} = \begin{bmatrix} h_f - h' \\ V_f - V' \\ \gamma_f - \gamma' \end{bmatrix} = 0. \tag{37}$$

Notice that the final time t_f and final downrange x_f are unknown. The coast time and the burn time of the last stage are not specified for this problem, as they are included in the objective function and their optimal value is obtained through the PSO algorithm. Hence, the transversality condition is given (Pontani 2014) by

$$H_f^{\text{last stage}} + H_f^{\text{coast}} - H_0^{\text{last stage}} = 0\,, \tag{38}$$

with $H_f^{\text{last stage}} < 0$.

To handle the trajectory constraints and the transversality condition, we use a static penalty functions to transform the problem into an unconstrained minimization to be solved by the PSO algorithm. The original objective function J is penalized if the rocket does not reach the required altitude, velocity, or flight path angle and if the transversality condition is not verified. The augmented objective function is then given by

$$\begin{aligned} J' =& J + \sum_{c=1}^{3} s_c \left\| x_{c,f} - x_{c'} \right\| \\ &+ s_4 \left\| H_f^{\text{last stage}} + H_f^{\text{coast}} - H_0^{\text{last stage}} \right\| + C, \end{aligned} \tag{39}$$

where s_c denotes the constraint weight factor, $\boldsymbol{x}_f$ is the final state vector, and $\boldsymbol{x'}$ is the required state vector. The additional penalty term C accounts for the imposed trajectory constraints, being defined as

$$C = \begin{cases} 0 & \text{if trajectory constraints are not violated} \\ 10^20 & \text{if trajectory constraints are violated} \end{cases}. \tag{40}$$

This way, the optimizer will implicitly drive the solution toward the feasible region to avoid the penalties to the objective function that would occur if the constraints were violated.

4.2 MDO architecture and optimization algorithms

Designing a launch vehicle concerns several engineering disciplines, namely, aerodynamics, propulsion, structure, weight and sizing, costs, and trajectory. MDO allows the coupling of the rocket design and trajectory optimization, making it suitable for the integrated space launchers design.

The most common MDO architecture for general design optimization is the multidisciplinary design feasible (MDF) (Balesdent 2011), which consists of a single-level optimization formulation, requiring only one optimizer at the system level and a multidisciplinary design analysis (MDA). The MDA solves the interdisciplinary coupling equations at each iteration of the optimization process, guaranteeing that disciplines are consistent, that is, the coupling variables among disciplines are converged at each point of the design space. At the end of each MDA, the optimizer evaluates the design

performance and verifies if the solution is feasible, that is, complies with all given constraints.

The convergence of the MDA is typically obtained using fixed-point iteration (FPI) methods (Kodiyalam 1998) that provide higher robustness at the cost of lower convergence rate when compared to Newton methods. FPI methods include nonlinear Gauss–Seidel, where each discipline is solved sequentially given updated values from previous disciplines, and Jacobi, where the discipline analyses are solved in parallel using discipline values from previous iteration (Schumacher et al. 2017). Since the Jacobi approach does not updated the discipline variables as soon as they are computed, it requires more iterations (Cervera et al. 1996), so it only advantageous if discipline parallel analyses are performed.

As implied in the general coupled rocket preliminary design and trajectory optimization procedure flowchart in Fig. 1, there are two sub-problems: the rocket design and the rocket trajectory and control, each implying an optimization approach. We defined our architecture as multilevel, where the top-level optimizer is responsible for the structural sizing using the mass model while guaranteeing the trajectory requirements. The mass model itself implies an iterative process that is accomplished by a Gauss–Seidel FPI method for robustness and fast convergence. A bottom-level optimizer is used inside for the optimal trajectory and control, where an hybrid direct/indirect method is used: first, a direct method using an NLP problem formulation is used to obtain a fast solution of the trajectory parameters; then, these parameters are then used as initialization of the indirect method using the PMP to obtain an accurate solution.

The details about the search of the design space for each of the optimization levels are specific to the numerical algorithm used. Due to trade secrets, little information is available regarding design numerical design tools used in the space industry. While gradient-based algorithms are known to be used to optimize continuous design variables, optimal discrete variables are typically determined using a time-consuming, exhaustive search approach, where the systems are optimized assuming certain discrete values and the process repeated for all different combinations of allowable discrete values.

The complexity of a launch vehicle design space, involving several continuous and discrete variables, is a source of motivation to develop advanced optimization tools. Over the last two decades, there has been an increasing interest in heuristic approaches, which are typically inspired by natural phenomena and well suited for discrete optimization problems. The genetic algorithm (GA) (Deb et al. 2002) and the Particle Swarm Optimization (PSO) (Eberhart and Kennedy 1995) have been widely used in space industry for both design and trajectory optimization (Rafique et al. 2011; Vinkó and Izzo 2008). Both algorithms have been adopted in our design, corresponding to each different level of our two-level optimization approach, as described next.

4.2.1 Rocket design optimization algorithm

Genetic algorithms are inspired in Darwin's theory of evolution, by the inclusion of selection, crossover, and mutation techniques. A GA was developed in Python to optimize the vehicle design, allowing an easy implementation, parallel processing, and the possibility to explore a large design space and to improve the fitness of the solution candidates. The choice of a GA as a global optimizer allows the optimization of not only continuous variables, but also discrete variables, useful for the optimization of the number of stages/boosters and engines and the choice of Fuel/Oxidizer type. However, for the test cases in this paper, the implemented GA only performs continuous optimizations, thus fixing the number of discrete objects. The built-in parallelization option is based on the master-slave architecture shown in Fig. 5. The master node scatters the population individuals throughout the slave nodes to perform the individual fitness evaluation, later returning the information to the master node to create the next generation.

Details about the developed GA algorithm, including population initialization, selection, crossover and mutation operations, and benchmark against other implementations, can be found in "Appendix".

The rocket design is posed as a total mass minimization problem, where the fitness function corresponds to the rocket total mass, and is subjected to a penalty if the PSO algorithm is not able to find a sub-optimal trajectory for the current rocket individual. After the final rocket evaluation,

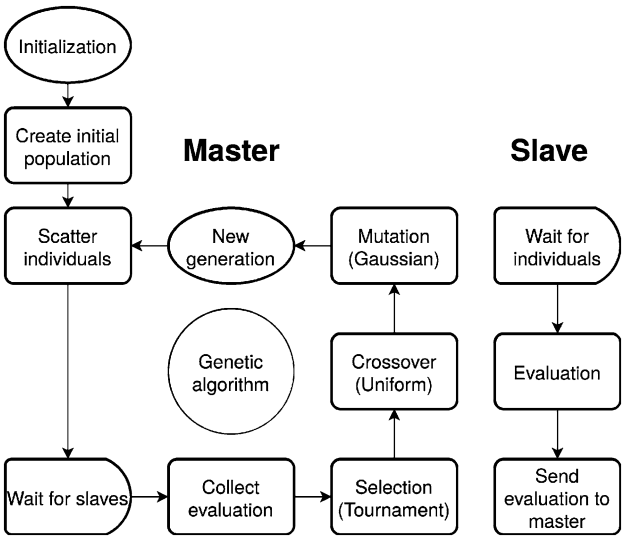

Fig. 5 Genetic algorithm implementation using master-slave architecture

the PSO proceeds to perform a more rigorous trajectory optimization, to increase orbit insertion accuracy. The design variables considered are the thrust and ΔV of each stage and the overall thickness and diameter of the rocket. The fitness function evaluation block in Fig. 5, performed by the slave nodes is detailed in Sect. 4.3.

4.2.2 Trajectory optimization algorithm

The design of launch vehicles is highly coupled with the calculated trajectory. The optimal trajectory is different for each feasible rocket and must be determined at each design iteration by the GA (refer to Fig. 6), assessing if the design configuration meets the performance requirements.

We chose a PSO algorithm to solve the NLP problem that optimizes the rocket trajectory, as it allows to accurately determine the required initial parameters used in indirect methods (Pontani 2014), while minimizing the required propellant mass used by the optimized rocket design for the specified mission. PSO algorithms model the social behavior of animal groups, using information obtained from each individual and from the swarm to reach the optimal solution. They are widely used in trajectory calculations due to their easy implementation and global search capability. We used the PSO algorithm available in the package PyGMO (Biscani and Izzo 2019) in Python.

The PSO algorithm provides the trajectory parameters required to find the optimal path. Each PSO particle is initiated with a parameter set represented by the unknown initial costate values (λ_{0h}, λ_{0V}, $\lambda_{0\gamma}$), the coast duration Δt_c and initialization time t_{ic}, last stage duration Δt_T and the pitch angle γ_p for the pitch maneuver. A trajectory simulation is then performed for each particle created by the PSO, until the rocket reaches orbit or when the maximum number of iterations is reached.

4.3 Framework implementation

The evaluation of the rocket total mass, representing the fitness function used by the GA algorithm presented in Sect. 4.2.1, follows the procedure graphically illustrated in Fig. 6.

At a high-level, the evaluation module can be divided in two main blocks: the rocket construction, where the total mass, mass build-up and sizing of the rocket are calculated, and the trajectory optimization block, where the optimal trajectory is calculated for the obtained design configuration. Following the penalty approach detailed in Sects. 2.3 and 4.1, the total mass is penalized whenever a design constraint or a trajectory constraint is not satisfied. This way, the GA algorithm will evolve the design so that the total mass estimate is kept as small as possible but large enough for the rocket to be structurally sound and meet the orbit insertion requirements.

The rocket construction block is detailed in Fig. 7, where the relevant input and output parameters are listed. It represents the implementation of our rocket mass and sizing model described in Sect. 3.1. The model takes as global input parameters the payload and the number of stages, whose value is prescribed according to the rocket mission type. The stage specific inputs—rocket type, diameter, wall thickness, velocity change ΔV, specific impulse, thrust-to-weight ratio, number of engines, propellant density and O/F ratio—can be either prescribed parameters or optimized variables. Additionally, rocket specific inputs—number of stages/boosters—can also be optimized by the implemented

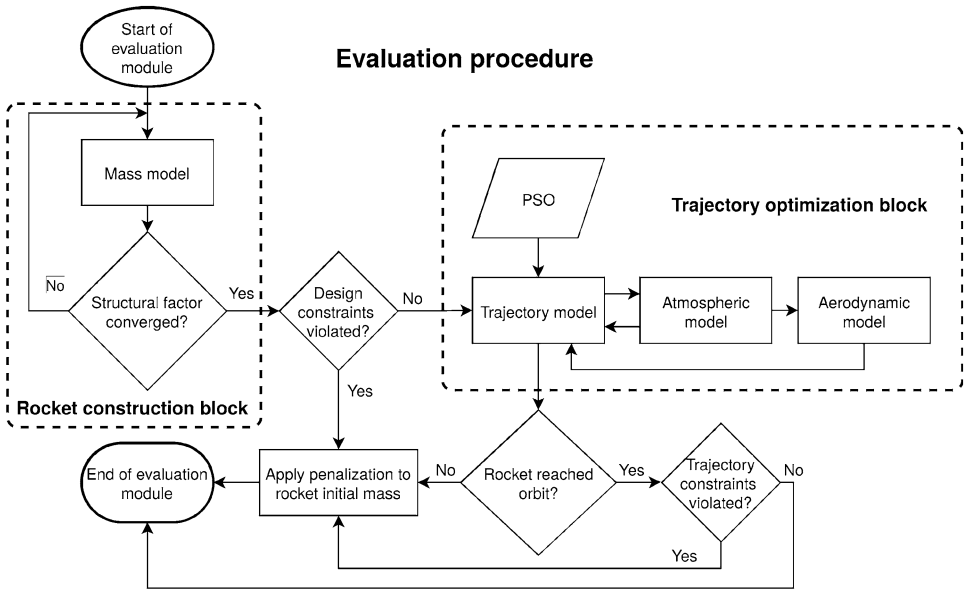

Fig. 6 Rocket construction and trajectory simulation flowchart

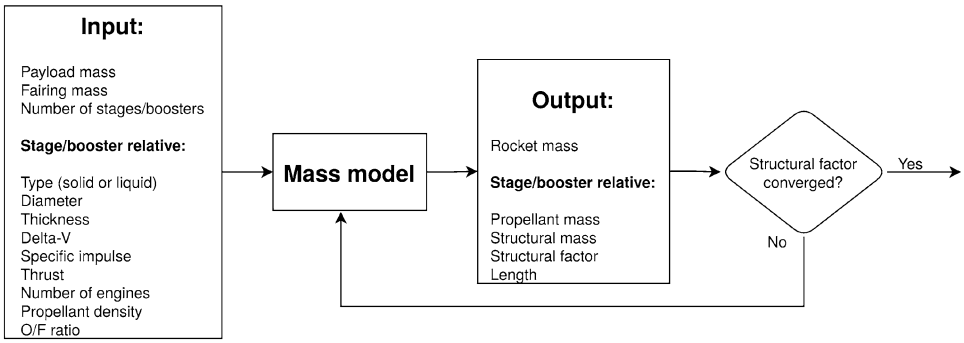

Fig. 7 Details of the rocket construction block data flow

GA algorithm. By using a fixed-point approach (see Sect. 4.2), the rocket mass is iterated until the structural factor is converged. Upon convergence, the mass model outputs the total rocket mass and its build-up: propellant and structural masses per stage, the structural factor and the length per stage. Thereafter, the high-level optimizer checks if all the design constraints are met (for instance, the total ΔV of the rocket is within the specified interval or the first-stage thrust is above the imposed lower limit). If the rocket meets all the requirements, the optimizer proceeds to the trajectory optimization block.

The trajectory optimization block in detailed in Fig. 8, where the relevant input and output parameters are listed. This block uses as inputs the outputs from the mass model, together with the trajectory initial and final conditions, that are prescribed according to the launch pad location and the orbit insertion point. The trajectory model solves the optimal control problem described in Sect. 4.1, where the optimal trajectory is calculated applying the PSO algorithm. The algorithm will try to find the initial pitch angle to start the gravity turn, the duration and initialization time of the coast phase, the thrusting time of the upper stage and the optimal adjoint variables to control the thrust direction in order to solve Eq. (38). During the trajectory simulation, the aerodynamic and atmospheric models described in Sect. 3.2.3 are used. The optimal trajectory found is expressed in terms of state variables (position and velocity), mass, velocity loss, structural forces, dynamic pressure, acceleration and thrust vector data. Afterward, the difference between the rocket final position and the mission objectives is used as a fitness function and fed into the GA fitness function [see Eq. (28)]. Additionally, some of parameters calculated through the trajectory model are used in the design constraints by the GA algorithm, such as the buckling critical stress (Sect. 3.1.2) and maximum acceleration (Sect. 3.2.2) conditions.

The developed modular framework described in Fig. 6 is represented in the Design Structure Matrix format (Lambe and Martins 2012) in Fig. 9 so that the coupling between both optimization blocks—rocket design and rocket trajectory, and their corresponding analyses modules, are highlighted in a concise view.

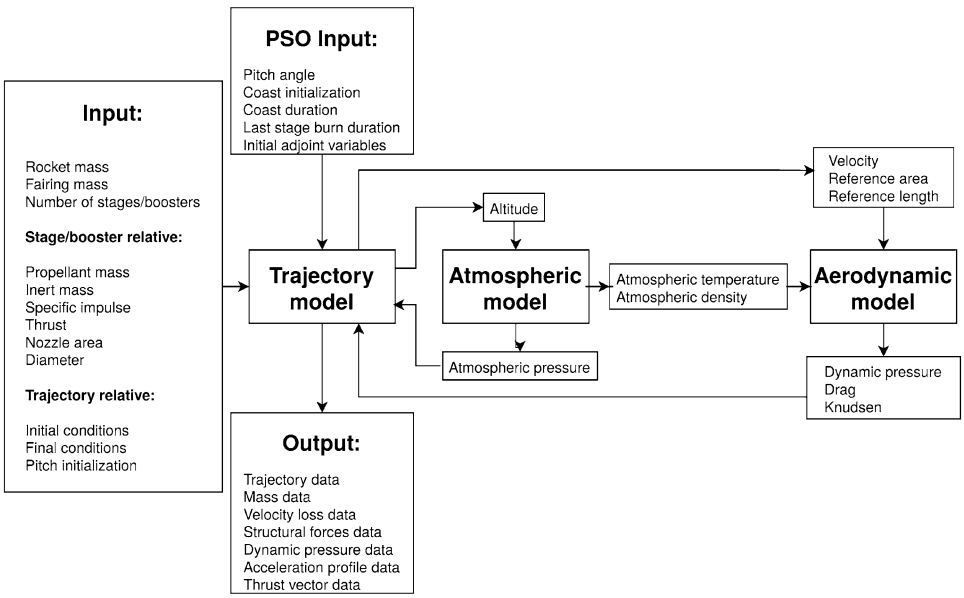

Fig. 8 Details of the trajectory optimization block data flow

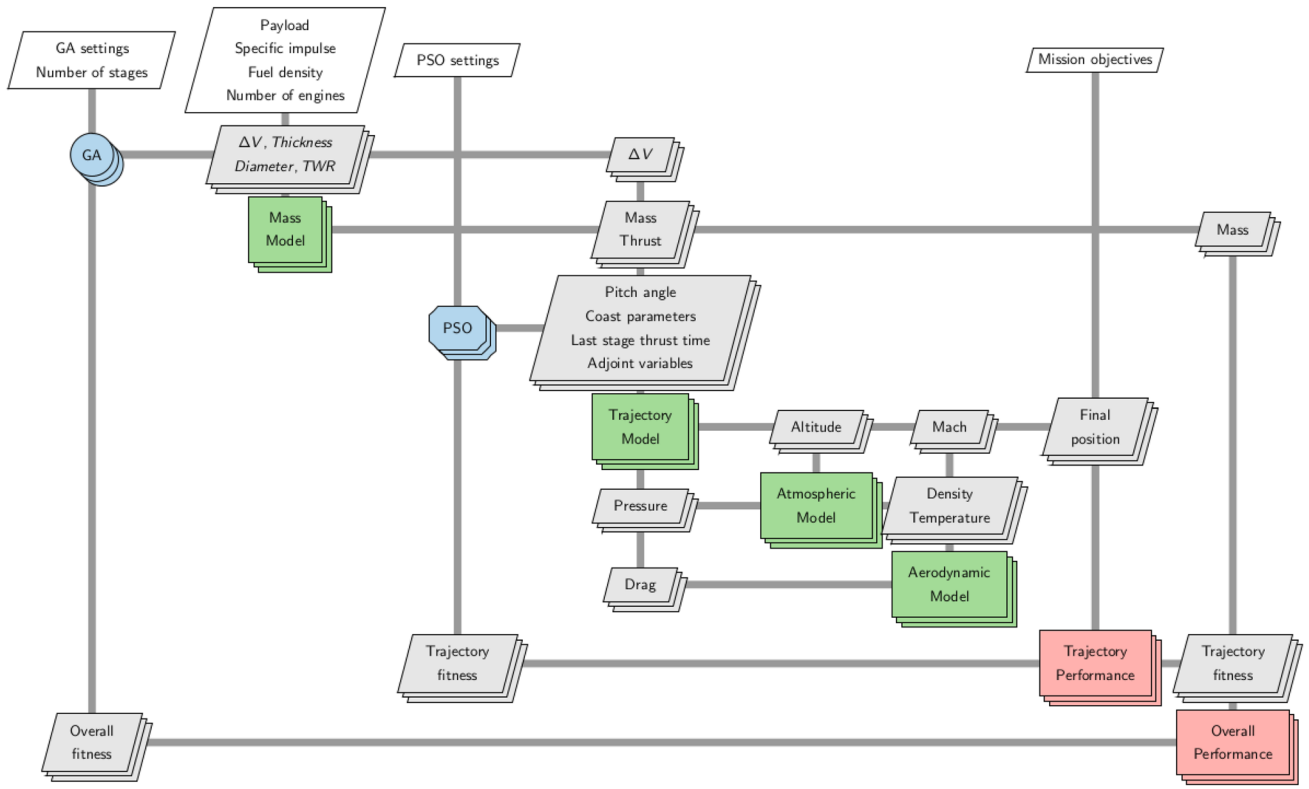

Fig. 9 Coupling relationship between disciplines using the Design Structure Matrix

Table 1 Summary of optimization problem components

Rocket design	
Optimizer	GA
Objective function	Rocket total mass
Constraints	$8000 < \Delta V < 11,000$
	$(T/W)_{\text{1st stage}} > 1.2$
	Mission completes
Design variables	Diameter
	ΔV
	Thickness
	T/W
	Number of stages*
	Number of engines*
	Number of boosters*
	Fuel type*
Rocket trajectory	
Optimizer	PSO
Objective function	J′ [Eq. (39)]
Constraints	Avoids ground
	Stress below maximum
Design variables	Adjoint variables
	Initial pitch angle
	Coast phase duration
	Coast phase starting time wrt start of last stage
	Last stage thrusting duration

*Available but not used in this work

Table 2 Proton-K rocket parameters (Proton 2009)

Proton-K	1st stage	2nd stage	3rd stage
Stage type	Liquid	Liquid	Liquid
Diameter [m]	5.4	4.1	4.1
Total mass [kg]	450,410	167,863	50,747
Propellant mass [kg]	419,410	156,113	46,562
Thrust [N]	10,450,000	2,324,970	608,220
Specific impulse [s]	316	327	327
Fuel density [kg/m^3]	793	793	793
Oxidizer density [kg/m^3]	1450	1450	1450
O/F ratio	2.67	2.67	2.67
Number of engines	6	4	1
Wall thickness [mm]	9	9	9
Payload mass [kg]			19,760
Fairing mass [kg]			2000

The design variables, constraints and objectives of the multilevel, multidisciplinary optimization problem, previously described in detail, are summarized in Table 1.

5 Models quality assessment

Before conducting any design optimization using our integrated framework, we individually assessed the quality of both the mass model (Sect. 5.1) and the trajectory model (Sect. 5.2) by comparing their estimates with data of an existing rocket.

5.1 Mass model estimate

We used the Proton-K rocket (Proton 2009) to assess the reasonability of the adopted mass model presented in Sect. 3.1. The relevant rocket parameters are listed in Table 2.

The comparison between the real values and our mass model estimates are presented in Table 3 for the rocket mass and Table 4 for the rocket sizing.

The registered maximum deviation occurs for the second-stage inert mass, with a difference of 3.74%, possibly explained by the underestimation of the propellant mass. The predicted propellant mass of each stage is just slightly lower than the real mass, always below 0.71% deviation. Thus, the rocket predicted total mass of each stage is remarkably similar to the real rocket mass, with deviations of less than 0.72%.

The estimated dimensions from the model in Table 4 are smaller than the real length, with a maximum relative deviation of 4.6%. The sizing model tends to have higher deviations for top stages. However, the first stage has the second highest error, possibly explained by the larger tanks diameter comparatively to the remaining stages.

Table 3 Comparison of mass estimate for the Proton-K rocket

	Mass	Real [kg]	Model [kg]	Deviation (%)
Fairing + Payload	Total	21,760	21,760	–
3rd stage	Propellant	46,562	46,460	− 0.22
	Inert	4185	4128	− 1.36
	Total	72,507	72,348	− 0.22
2nd stage	Propellant	156,113	155,006	− 0.71
	Inert	11,750	11,311	− 3.74
	Total	240,370	238,665	− 0.72
1st stage	Propellant	419,410	418,501	− 0.22
	Inert	31,000	32,117	+ 3.60
	Total	690,780	689,283	− 0.22

Table 4 Comparison of length estimate for the Proton-K rocket

	Real [m]	Model [m]	Deviation (%)
3rd stage	6.5	6.2	− 4.6
2nd stage	14	13.9	− 0.7
1st stage	21.2	20.9	− 1.4

Table 5 Mission requirements for the Proton-K rocket trajectory estimate

Payload mass [kg]	19,760
Altitude [m]	700,000
Velocity [m/s]	7037
Flight path angle [rad]	0.0

Table 6 PSO parameters for trajectory estimate

Coast time [s]	0 to 2000
Pitch angle [rad]	1.54 to 1.57
Adjoint variables	− 1.0 to 1.0
Last stage duration [%]	0 to 100
Coast start [%]	0 to 100

Due to the fairly small difference between the real rocket values and the model estimated values, we found the mass model to be acceptable for mass and sizing calculation of liquid rockets, so we incorporated it in our preliminary design optimization tool.

5.2 Trajectory model estimate

The trajectory model presented in Sect. 3.2 was also tested using the Proton-K rocket data in Table 2. We considered the rocket mission to deliver the payload to a circular orbit at 700 km of altitude and it is assumed to perform a vertical lift-off from the Vega Launch Complex (SLV) in Kourou,

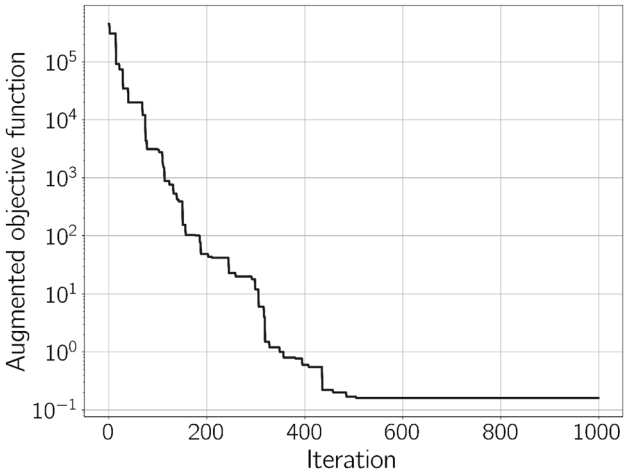

Fig. 10 Trajectory augmented objective function PSO history

French Guiana, located at a latitude of 5°. The launch location provides a eastward boost due to Earth's rotation of 463 m/s and this value was subtracted from the final orbital speed requirement (Fortescue et al. 2011). The Proton-K mission requirements are summarized in Table 5.

The parameter bounds for the PSO optimization are shown in Table 6. The pitch angle is kept close to 90° such that the lateral loads are reduced, as explained in Sect. 3.2. The last stage duration is given as a percentage of the time taken to deplete all the propellant, and the coast start is given as a percentage of the last stage flight duration (it provides the last stage thrusting time before starting the coast), since the coast phase only occurs during the last stage.

The PSO number of particles and maximum number of iterations are highly problem dependent so we started by testing the trajectory convergence using a relatively large number of particles (250) and iterations (1000) to ensure the algorithm reaches the optimal solutions (Shi and Eberhart 1999). The remaining parameters were tuned according to

Table 7 Optimal trajectory parameters and final state of the Proton-K rocket

PSO optimal solution	Coast time [s]	349
	Pitch angle [rad]	1.568
	Adjoint variable λ_h	-1.97×10^{-3}
	Adjoint variable λ_V	-9.15×10^{-1}
	Adjoint variable λ_γ	-9.96×10^{-1}
	Last stage duration [%]	98.86
	Coast start [%]	90.56
Final state	Altitude [m]	700,000
	Velocity [m/s]	7037.00
	Flight path angle [rad]	4.23×10^{-11}

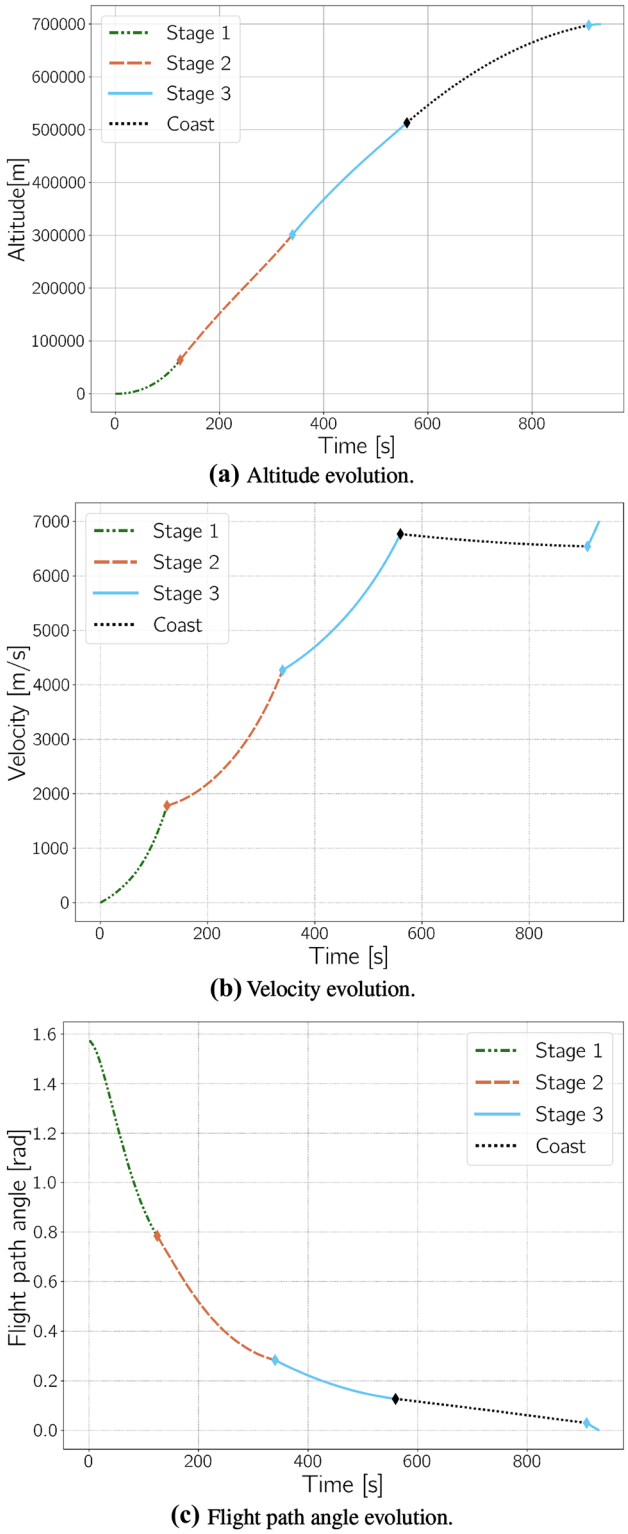

Fig. 11 Estimated Proton-K trajectory

Table 8 Mission requirements based on the Electron rocket

Payload mass [kg]	150
Altitude [m]	500,000
Velocity [m/s]	7612
Flight path angle [rad]	0.0

the PyGMO default values (Biscani and Izzo 2019), with cognitive parameter $c_1 = 2.05$, social parameter $c_2 = 2.05$, inertia weight $w = 0.7298$ and particle maximum velocity of 0.5 (normalized using its value amplitude).

The iteration history of the augmented objective function (39) for the best PSO particle is shown in Fig. 10. As observed, convergence was obtained relatively quickly, after 500 iterations, so both the number of particles and the maximum number of iterations are considered excessive and they can be safely reduced for the coupled design and trajectory optimization problem in Sect. 6 to further reduce the computational cost.

The PSO optimal solution and resultant final rocket state are summarized in Table 7, which confirms that the orbit insertion point conditions in Table 5 are satisfied.

The detailed altitude, velocity, and flight path angle evolution with time are shown in Fig. 11.

The Proton's real trajectory details are not publicly known so these results cannot be directly compared. However, it can be said that the estimated rocket position and velocity matches the expected qualitative evolution. The rocket takes 988 s to reach the specified final position, fully meeting the mission requirements specified in Table 5.

The altitude evolution, shown in Fig. 11a, demonstrates that the first stage is mostly responsible for the lift-off, being the subsequent stages used to gain both altitude and further velocity. During the coast phase, there is still a significant altitude gain due to the rocket momentum but it progressively goes to zero as the rocket turns horizontal to approach the desired circular orbit.

It is interesting to observe the velocity evolution in Fig. 11b, where the firing of each stage translates into a nearly quadratic behavior as a consequence of the active maximum acceleration constraint that forces the acceleration to be constant by throttling down the engine as the propellant mass is reducing. Notice also the final impulse required to reach the desired final velocity orbit insertion, that overcomes the velocity loss that occurred during the coast phase.

As for the flight path angle evolution in Fig. 11c, it shows that the rocket progressively turns from its initial vertical lift-off attitude to the final horizontal orbit insertion, being this change greater during the first stage where the gravity turn maneuver takes place.

Based on these results, we fell that the precision of the method used to calculate the optimal trajectory is attested.

Table 9 Trajectory parameters range for optimization using PSO

Coast time [s]	500 to 3000
Pitch angle [rad]	1.54 to 1.57
Adjoint variables	− 1 to 1
Last stage duration [%]	70 to 95 (100)
Coast start [%]	0 to 100

Table 10 Propulsive and propellant parameters

	1st stage	Other stages
TWR	1.2–2.0	0.8–1.5
Isp [s]	303	333
Nozzle diameter [m]	$0.6D_{\text{stage}}$	$0.9D_{\text{stage}}$
Fuel density [kg/m^3]	810	810
Oxidizer density [kg/m^3]	1142	1142
O/F ratio	2.61	2.61

Table 11 Design parameters

Rocket type	Liquid
ΔV/stage [m/s]	3000–6000
Diameter [m]	1.0–1.5
Wall thickness [mm]	2.0–5.0
Engines per stage	1

6 Preliminary design of a small launch vehicle

To demonstrate our developed coupled design and trajectory optimization procedure, we selected the mission of the small launcher Electron (Electron 2020) to be used as reference in the preliminary design of our launch vehicle (Sect. 6.1). Our coupled design and trajectory solution, using relatively simple models, is then compared to the real launcher (Sect. 6.2).

6.1 Problem setup

The optimization problem focus on optimizing two rockets, one with a 5% reserve of propellant and the other without any reserve. The propellant reserve, intended to provide a safety margin for engine malfunction, is done by imposing an upper limit of 95% on propellant consumption in the last stage.

The Electron mission requirements (Electron 2020), summarized in Table 8, are the basis for the design to be produced by our optimization framework driven by the GA algorithm.

Table 12 Genetic algorithm parameters

Maximum generations	30
Number of individuals	50
Crossover rate	0.75
Mutation rate	$0.5e^{-0.025gen_k}$
Step-size	$1.0e^{-0.075gen_k}$

Table 13 Particle swarm optimization parameters

Maximum iterations	250/1000
Number of particles	100/250
Cognitive parameter	2.05
Social parameter	2.05
Inertia weight	0.7298

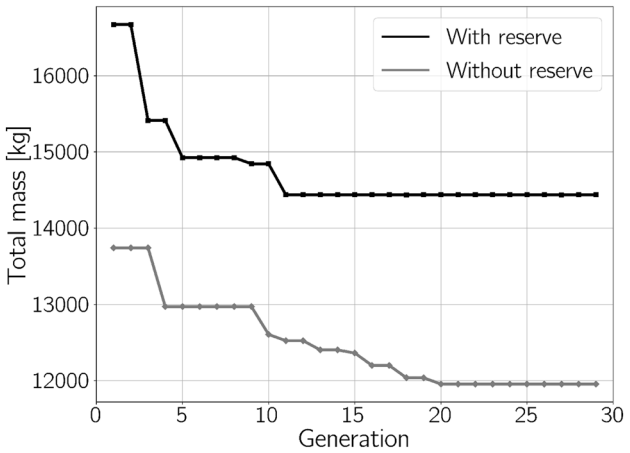

Fig. 12 Rocket best total mass evolution

The trajectory optimization parameters, used by the PSO algorithm in the trajectory model, are shown in Table 9. These were slightly adjusted compared to the ones used in Sect. 5, particularly the expected longer coast time and the last stage duration toward the end of the mission.

In our work, the Thrust-to-Weight ratio (TWR) was limited to $1.2 \leq \text{TWR} \leq 2$ to guarantee the successful rocket ascent and preventing the first stage to have too much thrust, avoiding unnecessary aerodynamic loads. This interval was selected using the previous knowledge that a TWR outside the range would lead to failed design caused by mission and structural constraints and it is aligned with typical values for large rockets, where a larger TWR, is hard to achieve and leads to excessive accelerations near the burnout of the stage. Additionally, using this knowledge to limit the TWR reduces the design space, thus reducing the convergence time and increasing the number of feasible designs in the GA population. The Electron TWR is ~ 1.76 (Electron 2020), which resides inside the imposed interval. For a direct comparison between our developed designs and the Electron rocket, we kept the specific impulse, the number of stages and the propellant restricted to the real rocket parameters. The specified propulsive parameters are listed in Table 10.

Table 14 Optimal design parameters of the two-stage rocket

Stage	With 5% reserve		Without reserve	
	1st	2nd	1st	2nd
ΔV [m/s]	4233	5455	3434	5832
TWR	1.70	0.99	1.79	0.87
Thickness [mm]	2.00	2.00	2.00	2.00
Diameter [m]	1.03	1.03	1.02	1.02
Propellant mass [kg]	11,029	1971	8166	2363
Inert mass [kg]	1068	263	916	282
Fairing mass [kg]		44		44
Total mass [kg]	14,525		11,922	

The design parameters and allowable ranges are shown in Table 11. Liquid propellant engines are used, similarly to the real rocket. The variable bounds are choose such that the ranges encompass the real rocket values but still provide us sufficient design freedom. For simplicity, the diameter and wall thickness are assumed equal for all stages. It is worth noting that the Electron wall thickness is not public knowledge and therefore not known if within the considered range. The material chosen for both tank walls and for the rocket walls is a carbon fiber composite, with density $\rho_{\text{mat}} = 1700\ \text{kg/m}^3$. Additionally, instead of changing the number of engines per stage, each stage is restricted to one engine and the TWR is optimized, since the required propulsion is unknown. Naturally, all these simplifications directly affect the estimated rocket mass.

The GA algorithm parameters are summarized in Table 12, where the step-size is normalized with the boundary width. The optimization was performed with a population of 100 individuals along 30 generations, found sufficient as attested by the convergence history in Fig. 12, and the remaining parameters were selected according to the optimal parameters obtained from tuning the GA.

For each individual design at each GA generation, a trajectory optimization using PSO is performed with 100 particles, as these have shown to be able to sub-optimize the trajectory within a maximum number of iterations of 250. The remaining PSO parameters were the default values provided by the PSO algorithm from PyGMO, as listed in Table 13. Early PSO convergence is assumed if the PSO algorithm finds the optimal trajectory within 0.1% deviation for the insertion altitude and velocity, and 0.0175 rad deviation for the final flight path angle.

A more accurate trajectory optimization is performed for the best candidate after the design optimization, using a

Table 15 Comparison of characteristics between the optimal designs and the Electron rocket

	With 5% reserve	Without reserve	Electron
Number of stages	2	2	2
Total mass [kg]	14,525	11,922	12,500
Diameter [m]	1.03	1.02	1.2
Length [m]	18.82	15.92	14.5
Number of engines	1/1	1/1	9/1

maximum number of iterations of 1000 with 250 particles, to confirm whether the selected design is able to actually able perform the orbit insertion.

6.2 Resulting optimal design

We run our coupled rocket preliminary design and trajectory optimization procedure on a cluster with 13 Intel Xeon E312xx (Sandy Bridge) 2 Ghz processor nodes, with four cores each. It took 2.18 h wall time to find the optimal solution for the rocket without propellant reserve and 2.38 h for the one with 5% reserve, having the algorithm converged well within the maximum number of generations as seen in Fig. 12.

It is clear that including the propellant reserve, despite being only 5%, has a great impact on the optimal two-stage rockets design, as seen in Table 14. We observe that the wall thickness and rocket diameter tend to the lower bound values to minimize the structural mass. We decided not to decreased the minimum allowed thickness to keep the design realistic. In practice, the interior walls are often reinforced with stringers to improve the mechanical strength and the vibration behavior. As expected, the reserve propellant has a considerable impact on the total mass: the rocket with 5% propellant reserve has a significant higher mass than the rocket without propellant reserve, resulting in an additional 2503 kg, which represents a 22% increase. This higher mass contributes to a significantly lower ΔV with a deficit of 423 m/s comparing the second stage only. These results attest the very high sensitivity to mass in rocket design.

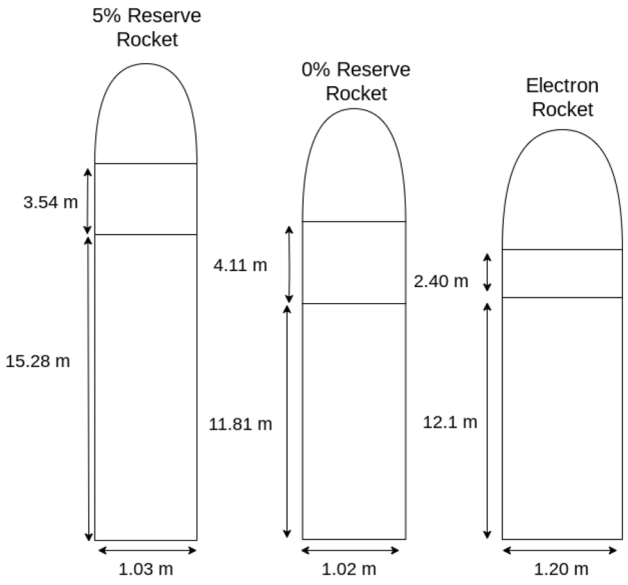

Fig. 13 Optimal designs and Electron rocket dimensions

The comparison between our optimally designed rockets and the Electron rocket is made in Table 15, where all meet the same mission requirements (Table 8) and are two-stage by imposition for direct comparison. The optimized rocket with propellant reserve presents a 16.2% increase in total mass and a 29.7% increase in length relatively to the Electron rocket, while the optimized rocket without propellant reserve presents a decrease in total mass of 4.6% but a 9.8% increase in length. Given the previously observed impact of the propellant reserve in our designs and noticing that the actual Electron total mass is bounded by our solutions, we may predict that the Electron rocket holds a propellant reserve lower than 5%, or divides the reserve by both stages, even though this is not information disclosed by the manufacturer.

An illustration of the dimensions of the three solutions can be found in Fig. 13. Regardless of the simplifications made, our designs are not drastically distinct from the real rocket, taking into account that it was not possible to compare all the design parameters. For example, a diameter constraint on the Electron can exist in order to better accommodate the payload. Also the Electron rocket is small and includes new technology which can make the mass model we used less adequate. The increase in length for both rockets is justified by the smaller diameter chosen by the optimizer to reduce the total mass, possibly as a consequence of the active thickness constraint. Also, our assumption for the walls material may have had some impact on the thickness and, consequently, on the overall dimensions.

The optimal trajectory parameters are listed in Table 16. Interestingly, there is no significant difference in the coast time between both designs. Also, both solutions keep the

Table 16 Rocket optimal trajectory parameters

	With 5% reserve	Without reserve
Coast time [s]	2637	2345
Pitch angle [rad]	1.566	1.564
Adjoint variable λ_h	-9.86×10^{-4}	-1.10×10^{-3}
Adjoint variable λ_V	-7.58×10^{-1}	9.99×10^{-1}
Adjoint variable λ_γ	-9.97×10^{-1}	-9.75×10^{-1}
Last stage duration [%]	95.0	99.9
Coast start [%]	98.7	99.2

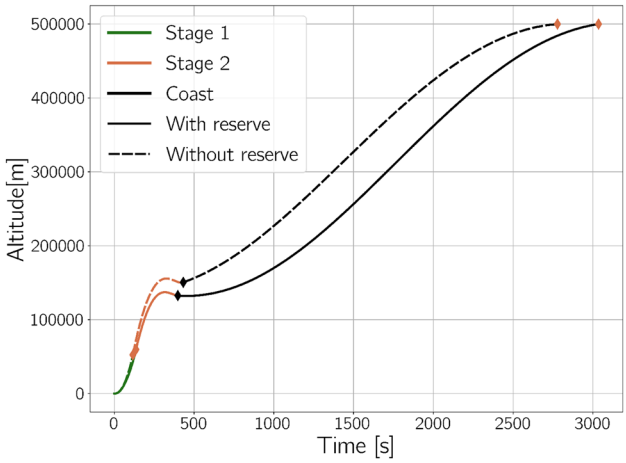

Fig. 14 Rocket optimal altitude evolution

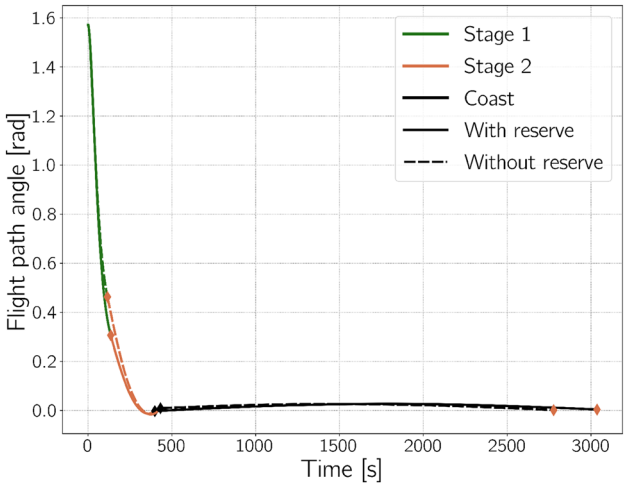

Fig. 16 Rocket optimal flight path angle evolution

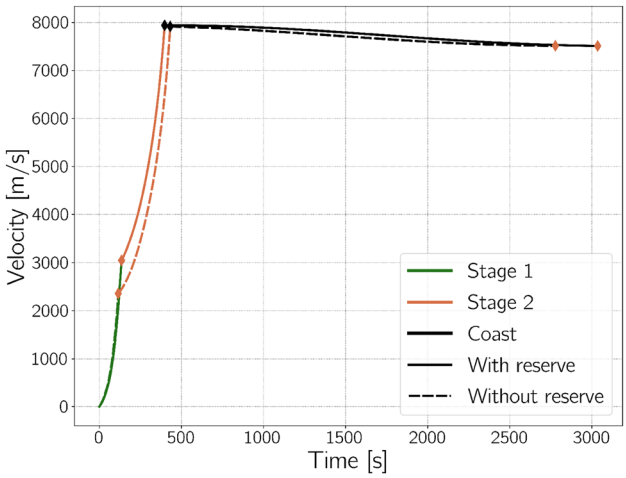

Fig. 15 Rocket optimal velocity evolution

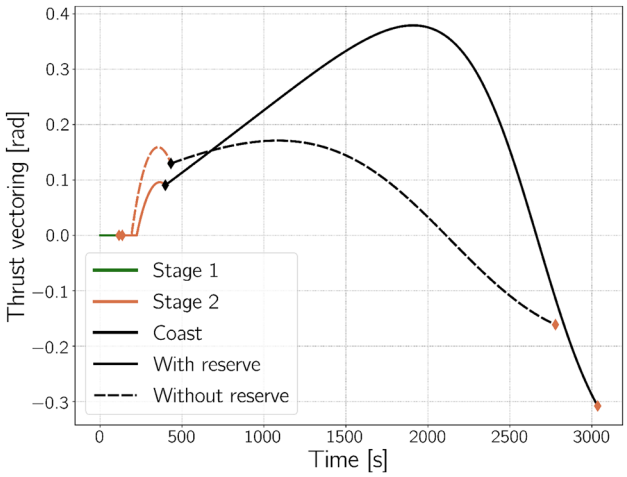

Fig. 17 Rocket optimal thrust vectoring evolution

pitch angle very close to 90° as desired. The non-zero adjoint variables indicate that their corresponding state equations (of motion) are being satisfied, according to optimal control theory. One clear difference between the rockets is in the last stage duration, where the optimizer rightfully found solutions that deplete all available propellant in order to minimize the rocket total mass: the last stage lasts until all the propellant is burnt (99.9%) for the solution without reserve; and it also burns as much as allowable (95.0%), keeping the required 5% reserve. As a consequence, the coast phase starts slightly sooner for the solution with propellant reserve, occurring near the end of the last stage for both rockets. We can infer from last line in Table 16 that the coast phase is followed by a short final impulse to reach orbit using just up to 1.3% and 0.7% of the last stage burn time, respectively, for the rocket with and without propellant reserve, as usual in circular orbit insertions.

The rocket altitude evolution with time is illustrated in Fig. 14. Comparing the design without propellant reserve with the one with 5%, the former exhibits a higher first-stage phase altitude gain due to its higher TWR, whose effect still extends to the second-stage phase despite the lower TWR. The latter then makes up during the coast phase as a consequence of its higher vertical velocity at the end of the second-stage burning. Both rocket configurations reach the required altitude with a time difference of 258 s.

The rocket velocity history is shown in Fig. 15. With the extension of the first stage, thanks to its higher stage propellant mass but despite its lower TWR, the design with 5% propellant reserve reaches a higher velocity before starting the second-stage phase. Before the coast phase, the rockets achieve their maximum velocity of 7900 m/s. Following the coast phase, both rockets achieve the required velocity for the circular orbit insertion (7612 m/s) as desired.

Table 17 Constrained parameter maximum values of optimal designs

Constraints		With 5% reserve	Without reserve
Acceleration [m/s^2]	≤ 5.00	5.00	5.00
Dyn. pressure [kPa]	≤ 55.0	51.0	50.1
Axial load [kN]	≤ 716	382	340

The two designs have a similar flight path angle evolution, as displayed in Fig. 16, and both follow the expected flight sequence depicted in Fig. 2. During lift-off, the angle is 90° for an initial vertical climb, but soon follows the gravity turn maneuver that progressively reduces such angle. The flight path angle is kept slightly positive during the entire coast phase to allow the rocket ascension to the desired orbit. It is worth noticing that, before the coast phase, the rockets turn horizontally for a brief moment to increase velocity and reduce gravity losses.

The thrust vectoring angle evolution is shown in Fig. 17. The rockets have a similar thrust vectoring angle evolution until the coast phase begins. During the first-stage firing, no vectoring is necessary since the turn is mostly initialized by the effect of gravity in the so-called gravity turn. After that, once the turn becomes significant and following the second-stage firing, it is notorious the trajectory control achieved with the thrust vectoring, slightly more in the rocket without reserve case. The control only starts after the jettison of the fairing, which happens at 224 s for the rocket with propellant reserve and at 187 s for the rocket without propellant reserve. Then, as soon as the coast stage begins, the thrust angle is not relevant since no stage thrusting is active. Finally, toward the very end of the mission when the short final impulse to reach orbit occurs, the thrust vectoring control becomes relevant again, and a negative value is now used to counteract the pitch and flight path angle so that a circular orbit insertion is achieved.

It is not possible to directly compare our optimal trajectories with the one performed by the Electron rocket since that data are not publicly available. Nevertheless, the main trajectory parameters shown in Figs. 14, 15, 16, 17 exhibit an evolution that is found quite plausible for multistage rockets.

As stated in Sect. 3.2.2, there are a number of constraints imposed to the trajectory to guarantee the safety of the rocket structure and its payload. The maximum registered values for acceleration, dynamic pressure and axial load are summarized in Table 17, where it can be confirmed that all are successfully handled by the optimizer.

As seen, the maximum allowable acceleration is limiting both designs, where the algorithm constrains both rocket accelerations, keeping it below $5g_0$. While the actual Electron maximum acceleration is unknown, this suggests that, if the payload allowed, increasing it would led to lighter rockets.

The dynamic pressure constraint is not active in our designs, as both rockets experience values below the admissible limit of 55 kPa. In addition, the axial load is also below the safety load of 716 kN for both cases, suggesting the reducing the allowable minimum wall thickness would further reduce the rockets total mass.

7 Conclusions

Our proposed procedure for the coupled rocket design and trajectory optimization demonstrated satisfactory performance, both in terms of the quality of the solutions and the affordable computational cost. The importance of coupling both disciplines was stressed as it is known that sequential optimization leads to sub-optimal results. To that end, our procedure guarantees that the rocket designed can execute the optimal trajectory given the mission requirements, while being the lightest possible, which indirectly translates into cheaper manufacturing (less material as a result of the lower empty weight) and lower operating costs (less propellant required).

Our developed genetic algorithm used as the main optimizer proved to be adequate for the intended parallel processing and the handling of the constraints, by means of penalties, and design variables types. Also, the PSO algorithm, chosen for the trajectory optimization sub-problem, performed quite well, as also verified in many other works.

The coupled optimal design and trajectory was implemented using relatively simple aerodynamic, structural and mass models that, despite having exhibited good accuracy, can be replaced, given our modular approach, with higher-fidelity models if enough computational power is available.

The procedure was demonstrated in the optimal design and trajectory of a small launch vehicle for a given representative mission, inspired on a state-of-the-art rocket. The solutions obtained compared quite well with the existing rocket, where the designs satisfy all imposed constraints.

It should be noticed that a coupled approach, such as the one we propose, is not suitable for the design of a generic multipurpose vehicle because the obtained solutions are the best for a specific mission profile expressed in terms of departure launch pad location and insertion orbit parameters.

Table 18 Optimization benchmark functions

Function	Dim.	Domain	Minimum $f(x^*)$ @ x^*
Sphere	20	$-5.12 \leq x_i \leq 5.12$	0 @ (0,...,0)
Rosenbrock	5	$-2.048 \leq x_i \leq 2.048$	0 @ (1,...,1)
Ackley	2	$-30 \leq x_i \leq 30$	0 @ (0,...,0)
Schwefel	10	$-500 \leq x_i \leq 500$	0 @ (420.97,...,420.97)
Rastrigin	10	$-5.12 \leq x_i \leq 5.12$	0 @ (0,...,0)

Table 19 Benchmark results of implemented GA

Function	Popul.	Gener.	Method	Minimum (average)	Time (average) [s]
Sphere	40	2000	Our GA	6.09e−9	2.91
			DEAP	5.22e−5	1.57
			PyGMO	3.06e−3	0.52
Rosenbrock	40	5000	Our GA	0.16	6.01
			DEAP	1.07	2.99
			PyGMO	0.67	1.92
Ackley	40	2000	Our GA	2.76e−4	2.25
			DEAP	1.29e−3	1.37
			PyGMO	1.48e−2	0.82
Schwefel	200	2000	Our GA	1.37e−4	13.13
			DEAP	2.62e−4	11.37
			PyGMO	4.28e−2	8.98
Rastrigin	100	5000	Our GA	1.01e−9	15.68
			DEAP	4.28	9.69
			PyGMO	3.51e−5	8.94

Appendix

A benchmark of developed GA algorithm

The population initialization was defined using a maximin Latin hypercube method, maximizing the smallest distance between any two design points, spreading them evenly over the entire design region (Husslage et al. 2006). The parents are selected through tournament, followed by an uniform crossover and a Gaussian mutation, creating the children for the next generation. The GA parameters were tuned using the Ackley function as objective function, to a crossover rate $p_c = 0.75$ and mutation rate $p_m = 0.5e^{-0.025gen_k}$, where gen_k is the generation number. The chosen step-size for the Gaussian mutation is $\lambda = 1.0e^{-0.075gen_k}$.

The developed GA was benchmark against the proved DEAP's GA (Fortin et al. 2012) and PyGMO's GA (Biscani and Izzo 2019), for the set of test functions listed in Table 18.

The benchmark results are summarized in Table 19, where the three algorithms used uniform crossover, tournament selection and Gaussian mutation throughout the generations. For a better comparison of the three algorithms, the crossover rate and the mutation rate chosen were $p_c = 0.75$ and $p_m = 0.2$, respectively, as suggested by Eiben et al. (1999) and Haupt and Haupt (2004). However, it is not possible to guarantee that DEAP and PyGMO do not internally change the parameters set at the beginning of the optimization to ease the search of the global minima. Therefore, to the best of the authors' knowledge, the most fair comparison was performed. The population size (Popul.) and the maximum number of generations (Gener.) were adjusted for each function.

As seen in Table 19, our developed GA algorithm exhibits a significantly better solution accuracy than DEAP and PyGMO, believed to be due to the better control of the Gaussian standard deviation required for the individual mutation. However, our GA presently requires a slightly higher computational time (up to 100% increase when compared to DEAP and to 460% increase when compared to PyGMO), but faster times can be achieved in future through the compilation of our implemented GA code. Additionally, our GA presents an easy-to-use interface, easily enabling the combined optimization of discrete and continuous variables. Observing these results, we confidently used our developed algorithm in the MDO rocket design procedure presented in this work.

Supplementary Information The online version contains supplementary material available at https://doi.org/10.1007/s00158-022-03285-y.

Acknowledgements The work of A.C. Marta and P.J.S. Gil was supported by FCT, through IDMEC, under LAETA, project UIDB/50022/2020.

Declarations

Conflict of interest On behalf of all authors, the corresponding author states that there is no conflict of interest.

Replication of results The results can be reproduced using the developed code and instructions that are made available as supplementary material to the manuscript.

References

Arias-Montano A, Coello CAC, Mezura-Montes E (2012) Multiobjective evolutionary algorithms in aeronautical and aerospace engineering. IEEE Trans Evol Comput 16(5):662–694. https://doi.org/10.1109/TEVC.2011.2169968

Balesdent M (2011) Multidisciplinary design optimization of launch vehicles. PhD thesis, Ecole Centrale de Nantes

Bayley DJ, Hartfield RJ, Burkhalter JE, Jenkins RM (2008) Design optimization of a space launch vehicle using a genetic algorithm. J Spacecr Rockets 45(4):733–740. https://doi.org/10.2514/1.35318

Bernstein KS (2011) Structural design requirements and factors of safety for spaceflight hardware. Technical report JSC 65828 Rev. A, NASA

Betts JT (1998) Survey of numerical methods for trajectory optimization. J Guid Control Dyn 21(2):193–207. https://doi.org/10.2514/2.4231

Biscani F, Izzo D (2019) esa/pagmo2: pagmo 2.10. https://doi.org/10.5281/zenodo.2529931

Braun RD, Kroo IM (1996) Development and application of the collaborative optimization architecture in a multidisciplinary design environment. In: Multidisciplinary design optimization: state of the art. SIAM, pp 98–116

Campos LMBC, Gil PJS (2018) On four new methods of analytical calculation of rocket trajectories. Aerospace. https://doi.org/10.3390/aerospace5030088

Campos LMBC, Gil PJS (2020) The two-point boundary-value problem for rocket trajectories. Aerospace. https://doi.org/10.3390/aerospace7090131

Casalino L, Masseni F, Pastrone D (2021) Hybrid rocket engine design optimization at politecnico di torino: a review. Aerospace. https://doi.org/10.3390/aerospace8080226

Cervera M, Codina R, Galindo M (1996) On the computational efficiency and implementation of block-iterative algorithms for nonlinear coupled problems. Eng Comput 13(6):4–30. https://doi.org/10.1108/02644409610128382

Chambre PA, Schaaf SA (2017) Flow of rarefied gases. Princeton University Press, Princeton Legacy Library. ISBN 9781400885800

Chunna L, Hai F, Chunlin G (2020) Development of an efficient global optimization method based on adaptive infilling for structure optimization. Struct Multidisc Optim 62(6):3383–3412. https://doi.org/10.1007/s00158-020-02716-y

Civek E (2014) Multistage launch vehicle design with thrust profile and trajectory optimization. PhD thesis, Middle East Technical University. https://doi.org/10.13140/RG.2.2.13871.02725

Conway BA (2010) The problem of spacecraft trajectory optimization. Cambridge aerospace series. Cambridge University Press, Cambridge, pp 1–15

Curtis H (2015) Orbital mechanics: for engineering students. Aerospace engineering. Elsevier Science, Amsterdam. ISBN 9780080470542

Darrin A, O'Leary B (2009) Handbook of space engineering, archaeology, and heritage. In: Advances in engineering series. CRC Press, Boca Raton. ISBN 9781420084320

Deb K, Pratap A, Agarwal S, Meyarivan TAMT (2002) A fast and elitist multiobjective genetic algorithm: NSGA-II. IEEE Trans Evol Comput 6(2):182–197. https://doi.org/10.1109/4235.996017

do Nascimento LGM, Araújo LM, da Silva Fernandes S, Shimote WK, Rapozo RR (2022) Hybrid optimization algorithm for preliminary design of multistage launch vehicles. J Braz Soc Mech Sci Eng. https://doi.org/10.1007/s40430-022-03384-3

Dresia K, Jentzsch S, Waxenegger-Wilfing G, Hahn RDS, Deeken J, Oschwald M, Mota F (2021) Multidisciplinary design optimization of reusable launch vehicles for different propellants and objectives. J Spacecr Rocket 58(4):1017–1029. https://doi.org/10.2514/1.A34944

Duranté N, Dufour A, Pain V, Baudrillard G, Schoenauer M (2004) Multi-disciplinary analysis and optimisation approach for the design of expendable launchers. In: 10th AIAA/ISSMO multidisciplinary analysis and optimization conference, Albany. https://doi.org/10.2514/6.2004-4441

Eberhart R, Kennedy J (1995) A new optimizer using particle swarm theory. In: Proceedings of the sixth international symposium on micro machine and human science, Nagoya, Japan. https://doi.org/10.1109/MHS.1995.494215

Eiben AE, Hinterding R, Michalewicz Z (1999) Parameter control in evolutionary algorithms. IEEE Trans Evol Comput 3(2):124–141. https://doi.org/10.1109/4235.771166

Electron (2020) Payload user's guide, version 6.5 edn. Rocket Lab, Long Beach

Federici L, Zavoli A, Colasurdo G, Mancini L, Neri A (2021) Integrated optimization of first-stage SRM and ascent trajectory of multistage launch vehicles. J Spacecr Rocket 58(3):786–797. https://doi.org/10.2514/1.A34930

Fortescue P, Swinerd G, Stark J (eds) (2011) Spacecraft systems engineering, 4th edn. Wiley, Hoboken. ISBN 9780470750124

Fortin FA, De Rainville FM, Gardner MA, Parizeau M, Gagné C (2012) DEAP: evolutionary algorithms made easy. J Mach Learn Res 13(70):2171–2175

Frank C, Pinon O, Tyl C, Mavris D (2015) New design framework for performance, weight, and life-cycle cost estimation of rocket engines. In: 6th European conference for aeronautics and space sciences, Krakow, Poland

Husslage BGM, Rennen G, van Dam ER, den Hertog D (2006) Space-filling latin hypercube designs for computer experiments. Optim Eng 12:611–630. https://doi.org/10.1007/s11081-010-9129-8

Garrido JV, Sagliano M (2021) Ascent and descent guidance of multistage rockets via pseudospectral methods. https://doi.org/10.2514/6.2021-0859

Hao Z, Hui T, Guobiao CB, Weimin B (2015a) Uncertainty analysis and design optimization of hybrid rocket motor powered vehicle for suborbital flight. Chin J Aeronaut 28(3):676–686. https://doi.org/10.1016/j.cja.2015.04.015

Hao Z, Hui T, Guobiao C, Weimin B (2015b) Uncertainty analysis and probabilistic design optimization of hybrid rocket motors for manned lunar landing. Sci China Technol Sci 58(7):1234–1241. https://doi.org/10.1007/s11431-015-5849-5

Hao Z, Haowen L, Pengcheng W, Guobiao C, Feng H (2020) Uncertainty analysis and design optimization of solid rocket motors with finocyl grain. Struct Multidisc Optim 62(6):3521–3537. https://doi.org/10.1007/s00158-020-02728-8

Hargraves CR, Paris SW (1987) Direct trajectory optimization using nonlinear programming and collocation. J Guid Control Dyn 10(4):338–342. https://doi.org/10.2514/3.20223

Haupt R, Haupt S (2004) Practical genetic algorithms. Wiley InterScience electronic collection. Wiley, New Jersey. ISBN 9780471671756

Humble R (1995) Space propulsion analysis and design. McGraw-Hill Companies, Incorporated, New York. ISBN 9780070313200

Kanazaki M, Yoda H, Chiba K, Kitagawa K, Shimada T (2017) Design methodology of a hybrid rocket-powered launch vehicle for suborbital flight. J Aerosp Eng. https://doi.org/10.1061/(ASCE)AS.1943-5525.0000778

Kim H, Rideout D, Papalambros P, Stein J (2003) Analytical target cascading in automotive vehicle design. J Mech Des 10(1115/1):1586308

Kliche D, Mundt C, Hirschel EH (2011) The hypersonic Mach number independence principle in the case of viscous flow. Shock Waves 21:307–314. https://doi.org/10.1007/s00193-011-0318-y

Kodiyalam S (1998) Evaluation of methods for multidisciplinary design optimization. Technical report CR-1998-208716, NASA

Koiter WT (1945) The stability of elastic equilibrium. PhD thesis, Techische Hooge School a Delft

Lambe AB, Martins JRRA (2012) Extensions to the design structure matrix for the description of multidisciplinary design, analysis, and optimization processes. Struct Multidisc Optim 46:273–284. https://doi.org/10.1007/s00158-012-0763-y

Li J, Peng K, Wang W, Wu Z, Zhang W (2021) Optimization design of rockoons based on improved sequential approximation optimization. Proc Inst Mech Eng G 236(1):140–153. https://doi.org/10.1177/09544100211008604

Maddock CA, Ricciardi L, West M, West J, Kontis K, Rengarajan S, Evans D, Milne A, McIntyre S (2018) Conceptual design analysis for a two-stage-to-orbit semi-reusable launch system for small satellites. Acta Astronaut 152:782–792. https://doi.org/10.1016/j.actaastro.2018.08.021

Mahjub A, Mazlan NM, Abdullah MZ, Azam Q (2020) Design optimization of solid rocket propulsion: a survey of recent advancements. J Spacecr Rocket 10(2514/1):A34594

Martins JRRA, Lambe AB (2013) Multidisciplinary design optimization: a survey of architectures. AIAA J 51(9):2049–2075. https://doi.org/10.2514/1.J051895

Meseguer J, Pérez-Grande I, Sanz-Andrés A (2012) Spacecraft thermal control (Woodhead Publishing in mechanical engineering). Elsevier Science, Amsterdam. ISBN 9780857096081

Okninski A (2017) Multidisciplinary optimisation of single-stage sounding rockets using solid propulsion. Aerosp Sci Technol 71:412–419. https://doi.org/10.1016/j.ast.2017.09.039

Pallone M, Pontani M, Teofilatto P (2016) Modeling and performance evaluation of multistage launch vehicles through firework algorithm. In: Proceedings of the 6th international conference on astrodynamics tools and techniques, Darmstadt, Germany

Pontani M (2014) Particle swarm optimization of ascent trajectories of multistage launch vehicles. Acta Astronaut 94(2):852–864. https://doi.org/10.1016/j.actaastro.2013.09.013

Pontryagin LS (1987) Mathematical theory of optimal processes (Classics of soviet mathematics). Taylor & Francis, London. ISBN 9782881240775

Proton (2009) Proton launch system mission planner's guide, revision 7th edn. International Launch Services, Reston, VA, lkeb-9812-1990

Qazi M, Linshu H (2006) Nearly-orthogonal sampling and neural network metamodel driven conceptual design of multistage space launch vehicle. Comput Aided Des 38(6):595–607. https://doi.org/10.1016/j.cad.2006.02.001

Rafique AF, He L, Kamran A, Zeeshan Q (2011) Hyper heuristic approach for design and optimization of satellite launch vehicle. Chin J Aeronaut 24(2):150–163. https://doi.org/10.1016/S1000-9361(11)60019-8

Reilly MH (1979) Equations of powered rocket ascent and orbit trajectory. Technical report NRL Report 8237, Naval Research Laboratory, Washington, DC

Ritter PA (2012) Optimization and design for heavy lift launch vehicles. Master's thesis, University of Tennessee—Knoxville

Rohrschneider RR (2002) Development of a mass estimating relationship database for launch vehicle conceptual design. Master's thesis, Georgia Institute of Technology

Ross IM, Fahroo F (2004) Pseudospectral knotting methods for solving nonsmooth optimal control problems. J Guid Control Dyn 27(3):397–405. https://doi.org/10.2514/1.3426

Schumacher A, Vietor T, Fiebig S, Bletzinger KU, Maute K (eds) (2017) Advances in structural and multidisciplinary optimization. In: Proceedings of the 12th world congress of structural and multidisciplinary optimization. Springer, Braunschweig

Sforza P (2011) Theory of aerospace propulsion. Aerospace engineering. Elsevier Science, Amsterdam

Shi Y, Eberhart RC (1999) Empirical study of particle swarm optimization. In: Proceedings of the 1999 congress on evolutionary computation (Cat. No. 99TH8406), Washington, DC. https://doi.org/10.1109/CEC.1999.785511

Shu JI, Kim JW, Lee JW, Kim S (2016) Multidisciplinary mission design optimization for space launch vehicles based on sequential design process. Proc Inst Mech Eng G 230(1):3–18. https://doi.org/10.1177/0954410015586858

Simpson T, Mauery TM, Korte JJ, Mistree F (2001) Kriging models for global approximation in simulation-based multidisciplinary design optimization. AIAA J 39(12):2233–2241. https://doi.org/10.2514/2.1234

Sobieszczanski-Sobieski J, Agte J, Sandusky R (1998) Bi-level integrated system synthesis. In: 7th AIAA/USAF/NASA/ISSMO symposium on multidisciplinary analysis and optimization, St. Louis, MO. https://doi.org/10.2514/6.1998-4916

Teixeira FACG, Gil PJS (2022) Rocket equation with burn losses and propellant tanks jettison. J Spacecr Rocket 59(2):685–690. https://doi.org/10.2514/1.A35201

Tewari A (2007) Atmospheric and space flight dynamics: modeling and simulation with MATLAB® and Simulink®. In: Modeling and simulation in science, engineering and technology. Birkhäuser, Boston. ISBN 9780817643737

Tewari A (2011) Advanced control of aircraft. Spacecraft and rockets, aerospace series. Wiley, Hoboken. ISBN 9781119972747

Tsuchiya T, Mori T (2004) Optimal conceptual design of two-stage reusable rocket vehicles including trajectory optimization. J Spacecr Rocket 41(5):770–778. https://doi.org/10.2514/1.1082

Turner MJL (2008) Rocket and spacecraft propulsion: principles, practice and new developments. Springer Praxis Books, Springer, Berlin, Heidelberg. ISBN 9783540692034

Vinkó T, Izzo D (2008) Global optimisation heuristics and test problems for preliminary spacecraft trajectory design. Technical report, ACT-TNT-MAD-GOHTPPSTD, European Space Agency, Advanced Concepts Team

Wei Z, Long T, Shi R, Tang Y, Li H (2019) Multidisciplinary design optimization of long-range slender guided rockets considering aeroelasticity and subsidiary loads. Aerosp Sci Technol 92:790–805. https://doi.org/10.1016/j.ast.2019.06.039

Wertz JR, Larson WJ (1999) Space mission analysis and design. Space technology library. Springer, Berlin. ISBN 9780792359012

Yao W, Chen X, Luo W, Tooren MV, Guo J (2011) Review of uncertainty-based multidisciplinary design optimization methods for aerospace vehicles. Prog Aerosp Sci 47(6):450–479. https://doi.org/10.1016/j.paerosci.2011.05.001

Zhang T, Yan X, Huang W, Che X, Wang Z (2021) Multidisciplinary design optimization of a wide speed range vehicle with waveride airframe and RBCC engine. Energy 235:121386. https://doi.org/10.1016/j.energy.2021.121386